ARMY RESEARCH LABORATORY

Three-Dimensional Correlation and Spectral Functions for Turbulent Velocities in Homogeneous and Surface-Blocked Boundary Layers

by David Keith Wilson

ARL-TR-1287

July 1997

The findings in this report are not to be construed as an official Department of the Army position unless so designated by other authorized documents.

Citation of manufacturer's or trade names does not constitute an official endorsement or approval of the use thereof.

Destroy this report when it is no longer needed. Do not return it to the originator.

Army Research Laboratory
Adelphi, MD 20783-1197

ARL-TR-1287 **July 1997**

Three-Dimensional Correlation and Spectral Functions for Turbulent Velocities in Homogeneous and Surface-Blocked Boundary Layers

David Keith Wilson
Information Science and Technology Directorate

Abstract

A pair of three-dimensional (3D) models for correlation functions and spectra of velocity fluctuations in turbulent boundary layers is presented. First, the case of homogeneous turbulence is considered. Von Kármán's energy spectrum is used to develop a complete set of 3D correlation and spectral equations. Second, it is shown how the homogeneous spectra can be modified to include the effect of eddy-blocking at the ground. Assuming that the disturbance to the turbulent flow resulting from the blocking is irrotational, an equation is developed that allows one to write the vertically inhomogeneous, 2D cross spectra as a function of the 2D cross spectra for a homogeneous flow. Although there are only two adjustable parameters in the inhomogeneous model, the variance and a length scale, the model is shown to agree quite well with a variety of previous results for the atmospheric convective boundary layer (CBL).

Contents

Figures

1. Introduction

Three-dimensional (3D) spectral and correlation models of turbulence in atmospheric boundary layers are required in a variety of applications, such as electromagnetic and acoustic wave propagation, turbulent transport and dispersion, response of structures exposed to the wind, and large-eddy simulation. In particular, the work described in this report is motivated by the need for good spectral models of large-scale turbulence in acoustical propagation applications.

It is not difficult to develop good 3D spectral and correlation models if one is interested only in small-scale *inertial subrange* turbulence (fig. 1). Owing largely to the work of Kolmogorov (1941), the spectral properties of the inertial subrange are well understood. The eddies belonging to the inertial subrange have spatial scales smaller than the instability generating the turbulence, and larger than the scales at which the turbulent kinetic energy is dissipated by viscosity. The large eddies generated directly by the instability belong to the *energy-containing subrange*, and the very small, dissipating eddies belong to the *dissipation subrange*.

For an atmospheric convective boundary layer (CBL), the energy input occurs at scales on the order of z_i, the inversion layer height, which is typically in the range from 0.5 to 2 km. Dissipation occurs on scales $\eta \sim 1$ mm. We see that there is an extremely broad inertial subrange in atmospheric turbulence, spanning five to six orders of spatial magnitude. Nonetheless, if turbulent

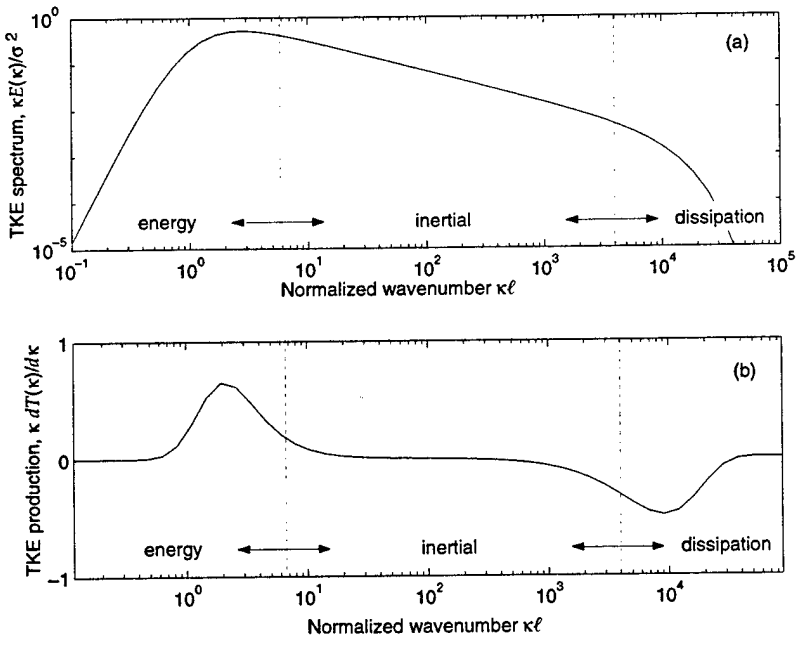

Figure 1: Three subranges of high-Reynolds-number turbulence. (a) Turbulent kinetic energy (TKE) spectrum, $\kappa E(\kappa)/\sigma^2$. (b) TKE production spectrum, $\kappa dT(\kappa)/d\kappa$. (App A gives actual equations plotted here.)

scales in either the energy-containing or dissipation subranges play a role in a given application, or if interactions between the eddies and ground surface (called *blocking* effects) are important, inertial subrange spectral modeling will fail.

In outdoor acoustic propagation, the wavelengths of interest can be as long as 30 m, and heights all the way down to ground level are important. Turbulent eddies having dimensions on the order of or greater than the wavelength primarily determine the scattered field. Hence classical inertial subrange scaling cannot be used in many acoustical applications, and models including the energy-containing subrange and ground blocking effects are required. Turbulent structure in the dissipation subrange is normally unimportant, though.

Despite the importance of having good 3D statistical models for atmospheric turbulence, previous experimental and modeling efforts have largely focused on single-point variances and 1D spectra taken in the direction of the mean wind. This is because such quantities can be determined from stationary towers. For 1D spectra, Taylor's frozen turbulence hypothesis is used to convert a time series recorded at the stationary tower to a spatial series. (Discussions of 1D spectral measurements and models are found in Kaimal *et al.* (1972), (1976), Højstrup (1982), and Panofsky and Dutton (1984).) Although single-point variances and 1D spectral models provide some basis and constraints on which to build a multidimensional model, they are not sufficient to fully define one.

In principle, by assuming homogeneity and isotropy, one could actually derive multidimensional spectra and correlation models solely from 1D turbulence measurements. The necessary relationships have been known for decades (Batchelor, 1953). Unfortunately, one cannot apply these relationships directly: atmospheric turbulence is known to be highly inhomogeneous and anisotropic, largely because of interactions with the ground.

Despite the inherent difficulties, some notable efforts have been made to develop multidimensional spectral/correlation models suitable for atmospheric turbulence. Kristensen *et al.* (1989) developed a general 3D model for turbulent velocity spectra in homogeneous, anisotropic boundary layers. Mann (1994) considered 3D spectra for turbulence generated by shear instabilities, allowing vertical inhomogeneities in his model. The work in this report builds on a spectral theory developed by Hunt and Graham (1978), who considered the effect of a boundary on turbulence in the absence of mean flow. As a result, the model here is intended for the atmospheric CBL. By this I mean that turbulence generation by convective instabilities (heating by the ground surface and the resulting density contrasts in the overlying air) dominates generation by shear instabilities (the wind blowing over the ground).

One of the principal benefits of building on Hunt and Graham's (1978) results is that the resulting spectral equations give the inhomogeneous, boundary-blocked spectra in terms of the spectra for homogeneous turbulence. Since the homogeneous case can be analyzed fully, as mentioned above, a complete spectral model results.

This report is divided into three main sections. Section 2 covers the case of homogeneous, isotropic turbulence. I provide some tutorial background for readers unfamiliar with this subject, and I develop a complete set of spectral/correlation equations for the homogeneous case. The main purpose of the section, however, is to derive the spectral results for homogeneous turbulence needed by the inhomogeneous, blocked model.

The inhomogeneous, blocked model is developed in section 3. I derive a general equation describing the blocking on 2D cross spectra, by assuming that the boundary does not modify the vorticity field. All other correlations and spectra can be determined from the 2D cross spectra by calculation of Fourier transforms.

Last, in section 4, I compare the inhomogeneous, blocked model to several experimental and computationally generated data sets, as well as to some previously developed models. Of course, as was discussed above, it is difficult to perform multidimensional correlation/spectral measurements in the atmosphere. However, quantities that are more easily measured, such as variances, integral length scales, and 1D spectra, are special cases of the full 3D correlation/spectral model, and I expect the model described here to behave well for these special, limiting cases. Hence it is quite worthwhile to test the model with measurements of these simpler quantities.

2. Correlation/Spectral Model for Homogeneous, Isotropic Turbulence

2.1 Preliminaries

Suppose we measure turbulent velocity fluctuations at two points in space. Let us indicate these two points as $\mathbf{x} = (x, y, z)$ and $\mathbf{x}' = (x', y', z')$. The coordinate system is oriented so that z is the vertical direction. Orientation of the horizontal axes is arbitrary, since I am not considering turbulence production by a mean horizontal wind shear in this report. The correlation function between the measured velocities is

$$R_{ij}(\mathbf{x}, \mathbf{x}') = \langle u_i(\mathbf{x}) u_j(\mathbf{x}') \rangle, \tag{2.1}$$

where the angle brackets indicate ensemble averaging, and u_i and u_j are the velocity fluctuations at the two points, oriented along the ith and jth coordinate axes (where x_1 is the same as x, $x_2 = y$, and $x_3 = z$).

By definition, in homogeneous turbulence, the correlation function depends only on the spatial separation between $\mathbf{x}$ and $\mathbf{x}'$. Hence we may write

$$R_{ij}(\mathbf{r}) = \langle u_i(\mathbf{x}) u_j(\mathbf{x}') \rangle, \tag{2.2}$$

where $\mathbf{r} = \mathbf{x}' - \mathbf{x}$.

The spectra are Fourier transforms of the correlation function. The Fourier transform convention used in this report is

$$\hat{f}(\kappa) = \frac{1}{2\pi} \int_{-\infty}^{\infty} f(r) \exp(-i\kappa r)\, dr \tag{2.3}$$

for the forward transform, and

$$f(r) = \int_{-\infty}^{\infty} \hat{f}(\kappa) \exp(i\kappa r)\, d\kappa. \tag{2.4}$$

for the inverse transform, in which κ is the wavenumber. For example, the 1D cross spectrum is

$$\Theta_{ij}(\kappa_1; r_2, r_3) = \frac{1}{2\pi} \int_{-\infty}^{\infty} R_{ij}(r_1, r_2, r_3) \exp(-i\kappa_1 r_1)\, dr_1. \tag{2.5}$$

By *cross* spectrum, I mean a spectrum involving two spatially separated points. The ordinary, single-point, 1D spectrum would be $\Theta_{ij}(\kappa_1; 0, 0)$. A cross spectrum can be thought of as a mixed spatial correlation/spectral function.

It is only a matter of convention that the Fourier transform was taken in the x_1-direction (i.e., with respect to r_1) in equation (2.5). Because of isotropy, we could have used either the x_2- or x_3-axis instead, and still had a complete set of 1D cross spectra. For example, consider the 1D cross spectrum with

Fourier transform in the x_3-direction $\Theta_{22}(r_\perp, r_\parallel; \kappa)$. Let us use the customary right-handed coordinate system, with the x_1-axis coming out of the page, x_2 to the right, and x_3 upwards. Looking in the direction of the velocity component (x_2-axis), we see the displacement $r_\perp$ to the right, the displacement $r_\parallel$ to the front, and the Fourier transform axis upwards. By reorienting ourselves so that we are looking down the x_3-axis with the x_2-axis to the right, we find the relationship $\Theta_{33}(\kappa; r_\perp, r_\parallel) = \Theta_{22}(r_\perp, r_\parallel; \kappa)$. Many other relationships follow similarly.

Besides the 1D cross spectra, I define 2D cross spectra $\phi_{ij}(\kappa_1, \kappa_2; r_3)$, and 3D spectra $\Phi_{ij}(\kappa_1, \kappa_2, \kappa_3)$, as follows:

$$\begin{aligned}\phi_{ij}(\kappa_1, \kappa_2; r_3) &= \frac{1}{4\pi^2}\int_{-\infty}^{\infty} R_{ij}(r_1, r_2, r_3)\exp(-i\kappa_1 r_1 - i\kappa_2 r_2)\,dr_1\,dr_2 \\ &= \frac{1}{2\pi}\int_{-\infty}^{\infty}\Theta_{ij}(\kappa_1; r_2, r_3)\exp(-i\kappa_2 r_2)\,dr_2, \end{aligned} \tag{2.6}$$

$$\begin{aligned}\Phi_{ij}(\kappa_1, \kappa_2, \kappa_3) &= \frac{1}{8\pi^3}\int_{-\infty}^{\infty} R_{ij}(r_1, r_2, r_3)\exp(-i\kappa_1 r_1 - i\kappa_2 r_2 - i\kappa_3 r_3)\,dr_1\,dr_2\,dr_3 \\ &= \frac{1}{2\pi}\int_{-\infty}^{\infty}\phi_{ij}(\kappa_1, \kappa_2; r_3)\exp(-i\kappa_3 r_3)\,dr_3. \end{aligned} \tag{2.7}$$

The eventual goal in these modeling efforts is to determine R_{ij}, Θ_{ij}, ϕ_{ij}, and Φ_{ij}. Of course, because of the Fourier transform interrelationships, only one of these functions is independent.

There are other useful symmetry relationships. Switching u_i and u_j in the definition of the correlation function, and applying homogeneity, we find

$$R_{ij}(r_1, r_2, r_3) = R_{ji}(-r_1, -r_2, -r_3). \tag{2.8}$$

Making use of this identity and the fact that R_{ij} is a real function, we find, from the Fourier transform definitions,

$$\Theta_{ij}(\kappa_1, \kappa_2, r_3) = \Theta_{ji}(-\kappa_1; -r_2, -r_3) = \Theta^*_{ji}(\kappa_1; -r_2, -r_3), \tag{2.9}$$

$$\phi_{ij}(\kappa_1, \kappa_2; r_3) = \phi_{ji}(-\kappa_1, -\kappa_2; -r_3) = \phi^*_{ji}(\kappa_1, \kappa_2; -r_3), \tag{2.10}$$

and

$$\Phi_{ij}(\kappa_1, \kappa_2, \kappa_3) = \Phi_{ji}(-\kappa_1, -\kappa_2, -\kappa_3) = \Phi^*_{ji}(\kappa_1, \kappa_2, \kappa_3). \tag{2.11}$$

2.2 Energy and Three-Dimensional Spectra

The starting point in developing correlations and spectra for homogeneous, isotropic turbulence is the 3D *turbulent kinetic energy* (TKE) spectral density $E(\kappa)$, where $\boldsymbol{\kappa} = (\kappa_1, \kappa_2, \kappa_3)$, and $\kappa = |\boldsymbol{\kappa}|$. (In the turbulence literature,

TKE usually implicitly refers to the TKE per unit mass. I adhere to that convention in this report.) $E(\kappa)$ is defined as the TKE per unit wavenumber magnitude. If one thinks of the TKE in 3D wavenumber space, $E(\kappa)$ is the energy in a shell of radius κ. Since the TKE spectral density at a given point in wavenumber space is $\Phi_{ii}(\boldsymbol{\kappa})/2$ (summation over repeated roman indices is implied), and the total energy in a shell of radius κ is $4\pi\kappa^2$ times that amount,

$$E(\kappa) = 2\pi\kappa^2\Phi_{ii}(\boldsymbol{\kappa}). \tag{2.12}$$

The total kinetic energy in the flow is

$$E = \int_0^\infty E(\kappa)\,d\kappa = \frac{1}{2}\int_{-\infty}^{\infty}\int_{-\infty}^{\infty}\int_{-\infty}^{\infty}\Phi_{ii}(\boldsymbol{\kappa})\,d\kappa_1\,d\kappa_2\,d\kappa_3. \tag{2.13}$$

The success of the correlation/spectral model depends on making a good choice for $E(\kappa)$. The main criteria are (1) it must agree well with data; and (2) it must be analytically convenient to manipulate. The following form for the 3D energy spectrum satisfies both criteria reasonably well within the energy-containing and inertial subranges (see app A):

$$E(\kappa) = \frac{4\Gamma(\nu+5/2)}{\sqrt{\pi}\Gamma(\nu)}\frac{\sigma^2\kappa^4\ell^5}{(1+\kappa^2\ell^2)^{\nu+5/2}}, \tag{2.14}$$

where σ^2 is the variance, κ the radial wavenumber, ℓ the length scale, Γ the gamma function, and ν sets the power law dependence in the inertial subrange ($\kappa\ell \gg 1$). With appropriate choices for σ^2, ℓ, and ν, equation (2.14) is equivalent to von Kármán's (1948) model for $E(\kappa)$. In particular, setting ν to $1/3$ results in Kolmogorov's $-5/3$ power law for the inertial subrange ($\kappa\ell \gg 1$). I will not explicitly set ν to $1/3$ until we obtain final results, since to do so would sacrifice generality without appreciably simplifying any of the spectral expressions.

Given the energy spectrum, it is a simple matter to determine the 3D spectra Φ_{ij}. One uses the following well-known formula, derived, for example, in Batchelor (1953):

$$\Phi_{ij}(\boldsymbol{\kappa}) = \frac{E(\kappa)}{4\pi\kappa^4}\left(\delta_{ij}\kappa^2 - \kappa_i\kappa_j\right). \tag{2.15}$$

2.3 Longitudinal Correlations and Spectra

As a next step, we could integrate the 3D spectra Φ_{ij} to find the 2D cross spectra ϕ_{ij}. It is somewhat more instructive, however, to first consider 1D spectra. Given equation (2.14), and the assumption of homogeneous, isotropic turbulence, it turns out that 1D spectral densities and correlation functions can be derived directly.

Let us begin with the 1D *longitudinal* autospectrum. By longitudinal, I mean that the velocity component is parallel to the direction of the wavenumber

axis: i.e., $\Theta_{11}(\kappa,0,0)$, $\Theta_{22}(0,\kappa,0)$, or $\Theta_{33}(0,0,\kappa)$. Note that isotropy implies that these three spectra are the same. Let us define a normalized, longitudinal spectrum as $\hat{f}(\kappa) = \Theta_{11}(\kappa,0,0)/\sigma^2$, which can be shown to be related to the energy spectrum as follows (Batchelor, 1953):

$$E(\kappa) = \sigma^2 \kappa^3 \frac{d}{d\kappa}\left[\frac{1}{\kappa}\frac{d\hat{f}(\kappa)}{d\kappa}\right]. \tag{2.16}$$

By integrating equation (2.16), it is straightforward to show that the normalized, longitudinal spectrum is

$$\hat{f}(\kappa) = \frac{\Gamma(\nu+1/2)}{\sqrt{\pi}\Gamma(\nu)} \frac{\ell}{(1+\kappa^2\ell^2)^{\nu+1/2}}. \tag{2.17}$$

The longitudinal spectrum is plotted as the solid line in figure 2, for $\nu = 1/3$.

We can derive the longitudinal correlation function $\sigma^2 f(r)$ by taking the inverse Fourier transform of equation (2.17). Using integral (3.771.1) in Gradshteyn and Ryzhik's (1994) tables, and the fact that the autospectrum is an even function, we find the normalized longitudinal correlation to be

$$f(r) = \frac{1}{2^{\nu-1}\Gamma(\nu)} \left(\frac{r}{\ell}\right)^{\nu} K_\nu\left(\frac{r}{\ell}\right), \tag{2.18}$$

where K_ν is the modified Bessel function of the second kind of order ν.

Since modified Bessel functions play an important role throughout the remainder of this report, it is worth taking a moment to discuss a couple of

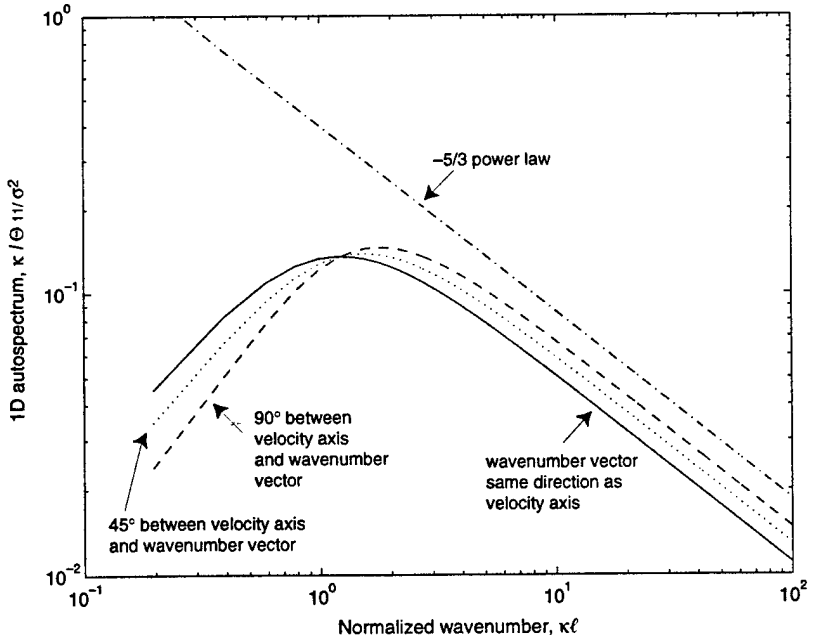

Figure 2: One-dimensional autospectral density model for $\nu = 1/3$.

their properties. For small arguments $\xi \ll 1$ and $\nu < 2$,

$$K\nu(\xi) \approx \frac{\Gamma(\nu)}{2}\left(\frac{\xi}{2}\right)^{-\nu} - \frac{\Gamma(1-\nu)}{2\nu}\left(\frac{\xi}{2}\right)^{\nu} + \frac{\Gamma(\nu)}{2(1-\nu)}\left(\frac{\xi}{2}\right)^{2-\nu}. \tag{2.19}$$

The leftmost of the three terms on the left is always the leading term in the series; the next most significant term in the series is either the second or third, depending on the particular value of ν. Substituting the first term into equation (2.18), it is easy to show that $f(0) = 1$, as it must. For large arguments $\xi \gg 1$, $K\nu$ becomes a decaying exponential:

$$K\nu(\xi) \approx \sqrt{\frac{\pi}{2\xi}}\exp(-\xi). \tag{2.20}$$

Equation (2.18) is plotted as the solid line in figure 3. It must be kept clear that $f(r)$ is the normalized autocorrelation only when the displacement is in the longitudinal direction. That is, $R_{11}(r,0,0) = R_{22}(0,r,0) = R_{33}(0,0,r) = \sigma^2 f(r)$. It is not generally true, even for an isotropic vector field, that $R_{11}(r,0,0)$ equals $R_{11}(0,r,0)$. The normalized *transverse* correlation function $g(r)$ is addressed in the next subsection.

2.4 Transverse Correlations and Spectra

So far, we have examined the autocorrelation and autospectral functions when the displacement (or the wavenumber component) is parallel to the direction of the velocity component. In order to study more general types of correlations, we need to develop an expression for the complementary case,

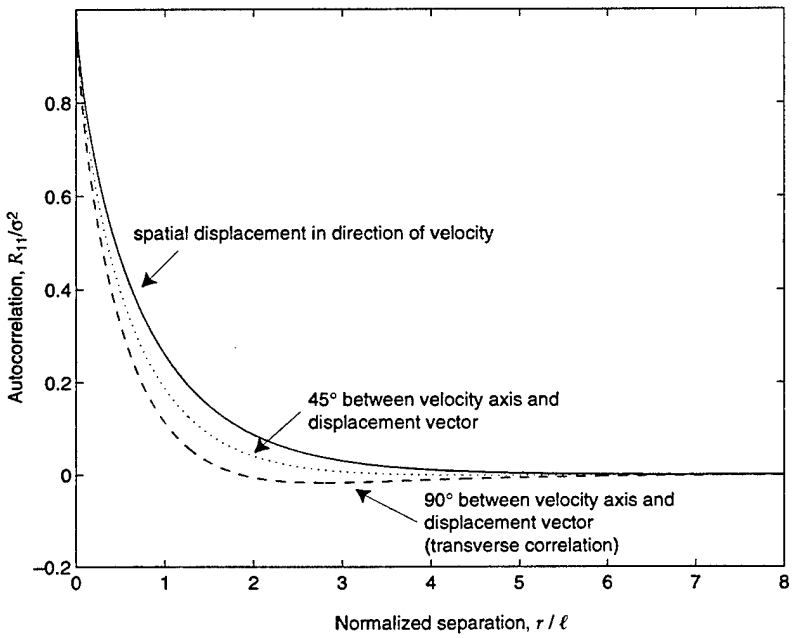

Figure 3: Autocorrelation function model for $\nu = 1/3$.

where the displacement is perpendicular to the velocity component. This is readily accomplished with the theory of isotropic vector fields in multiple dimensions, such as discussed in Batchelor (1953). For incompressible flow ($\partial u_i/\partial x_i = 0$), the transverse correlation $g(r)$ can be computed from the longitudinal $f(r)$ with the following formula (Batchelor, 1953):

$$g(r) = f(r) + \frac{r}{2}\frac{df}{dr}. \tag{2.21}$$

In this case, using equation (2.18), we find

$$\begin{aligned} g(r) &= \frac{1}{2^\nu \Gamma(\nu)} \left(\frac{r}{\ell}\right)^\nu \left[\frac{\nu+2}{\ell} K_\nu + \left(\frac{r}{\ell}\right) K'_\nu\right] \\ &= \frac{1}{2^{\nu-1}\Gamma(\nu)} \left(\frac{r}{\ell}\right)^\nu \left[K_\nu - \frac{1}{2}\left(\frac{r}{\ell}\right) K_{\nu-1}\right] \\ &= \frac{1}{2^{\nu-1}\Gamma(\nu)} \left(\frac{r}{\ell}\right)^\nu \left[(\nu+1)K_\nu - \frac{1}{2}\left(\frac{r}{\ell}\right) K_{\nu+1}\right]. \end{aligned} \tag{2.22}$$

(The argument of the modified Bessel functions is implicitly r/ℓ, unless otherwise specified.) In deriving the second and third forms above for $g(r)$, I made use of the differentiation formula for modified Bessel functions

$$K'_\nu(\xi) = -\frac{1}{2}\left[K_{\nu-1}(\xi) + K_{\nu+1}(\xi)\right], \tag{2.23}$$

and the recurrence relation

$$K_{\nu+1}(\xi) = K_{\nu-1}(\xi) + \frac{2\nu}{\xi} K_\nu(\xi). \tag{2.24}$$

Most generally, an isotropic, homogeneous vector field has a correlation tensor of the form (Batchelor, 1953)

$$R_{ij}(\mathbf{r}) = \sigma^2 \left[\frac{r_i r_j}{r^2} f(r) + \left(\delta_{ij} - \frac{r_i r_j}{r^2}\right) g(r)\right], \tag{2.25}$$

where r_i is the spatial separation along the ith axis, and $r^2 = r_1^2 + r_2^2 + r_3^2$. Using the final form in equation (2.22) for the transverse correlation, we obtain the full isotropic correlation tensor:

$$R_{ij}(\mathbf{r}) = \frac{\sigma^2}{2^{\nu-1}\Gamma(\nu)} \left(\frac{r}{\ell}\right)^\nu \left\{\frac{r_i r_j}{r^2} K_\nu + \left(\delta_{ij} - \frac{r_i r_j}{r^2}\right)\left[(\nu+1)K_\nu - \frac{1}{2}\left(\frac{r}{\ell}\right) K_{\nu+1}\right]\right\}. \tag{2.26}$$

Equation (2.26) is the complete correlation model for the velocity fluctuations in homogeneous, isotropic turbulence. It is plotted in figure 3 for $i = j$ and various angles between the displacement vector and the velocity. Note that the transverse correlation ($i = j$, with $r_i = r_j = 0$) actually becomes negative for large values of r/ℓ. Although this behavior may seem surprising initially, it is a physically necessary property of the transverse correlation (Batchelor, 1953), not just an artifact of using the von Kármán energy spectrum.

Finally, consider the normalized transverse spectral density function, which is the Fourier transform of $g(r)$. In the final form in equation (2.22), there are two terms, one involving K_ν and the other $K_{\nu+1}$. The Fourier transform of each term follows from (6.726.4) in Gradshteyn and Ryzhik's (1994) tables. After some algebra, we find

$$\hat{g}(\kappa) = \frac{\Gamma(\nu+1/2)}{\sqrt{\pi}\Gamma(\nu)} \frac{\ell}{(1+\kappa^2\ell^2)^{\nu+1/2}} \left(\nu + 1 - \frac{\nu+1/2}{1+\kappa^2\ell^2}\right). \tag{2.27}$$

To check equation (2.27), consider the inertial subrange limit $\kappa_1\ell \gg 1$. Then the term in brackets becomes $\nu + 1 = 4/3$. Comparison to equation (2.17) shows that $\hat{g}(\kappa) = (4/3)\hat{f}(\kappa)$ in the inertial subrange, a well-known result from the theory of isotropic vector fields (Panofsky and Dutton, 1984).

2.5 One-Dimensional Cross Spectra

We now have determined all the 1D *auto*spectra in free space. For example, $\Theta_{11}(\kappa,0,0) = \Theta_{22}(0,\kappa,0) = \sigma^2\hat{f}(\kappa)$, and $\Theta_{11}(0,\kappa,0) = \Theta_{22}(\kappa,0,0) = \sigma^2\hat{g}(\kappa)$. The other cases can be found by rotation of the coordinate axes. The next step is to find the 1D *cross* spectra, which we determine by transforming the correlation function (2.26). For concreteness, I take the direction of the Fourier transform to be the x_1 direction, and indicate the result using the following notation:

$$\Theta_{ij}(\kappa_1; r_2, r_3) = \frac{1}{2\pi}\int_{-\infty}^{\infty} R_{ij}(r_1, r_2, r_3)\exp(i\kappa_1 r_1)\, dr_1. \tag{2.28}$$

Consider first only the longitudinal part of the spectrum, the first term in equation (2.26). Defining $r_\perp^2 = r_2^2 + r_3^2$, we have the integral

$$\hat{f}(\kappa_1; r_2, r_3) = \frac{1}{\pi 2^{\nu-1}\Gamma(\nu)} \int_0^\infty \left(\frac{\sqrt{r_1^2+r_\perp^2}}{\ell}\right) K_\nu \left(\frac{\sqrt{r_1^2+r_\perp^2}}{\ell}\right) \cos(\kappa_1 r_1)\, dr_1. \tag{2.29}$$

This integral can be calculated in closed form; it is given as (6.726.4) in Gradshteyn and Rhyzhik's (1994) tables. We find

$$\hat{f}(\kappa_1; r_2, r_3) = \frac{\ell}{\sqrt{\pi}2^{\nu-1/2}\Gamma(\nu)} \left(\frac{\xi}{1+\kappa_1^2\ell^2}\right)^{\nu+1/2} K_{\nu+1/2}(\xi), \tag{2.30}$$

where $\xi^2 = (r_2^2 + r_3^2)(1+\kappa_1^2\ell^2)/\ell^2$.

The computation becomes somewhat more complicated when we include the transverse correlation, although results still can be obtained in closed form. Writing out the correlation function R_{11} as given by equation (2.26), and

simplifying with the recurrence formula (eq (2.24)), we find

$$R_{11}(r_1, r_2, r_3) = \frac{\sigma^2}{2^{\nu-1}\Gamma(\nu)} \left(\frac{r}{\ell}\right)^{\nu} \left[K\nu - \frac{r_\perp^2}{2\ell^2} \left(\frac{r}{\ell}\right)^{-1} K_{\nu-1}\right]. \tag{2.31}$$

The Fourier transforms of both terms in the square brackets are obtained readily. The first term integrates in the same manner as the longitudinal spectrum, whereas the second term has the same form if one replaces ν by $\nu - 1$. The result of the integration is

$$\Theta_{11}(\kappa_1; r_2, r_3) = \frac{\sigma^2 \ell}{\sqrt{\pi} 2^{\nu-1/2}\Gamma(\nu)} \left(\frac{\xi}{1+\kappa_1^2\ell^2}\right)^{\nu+1/2} \left[K_{\nu+1/2}(\xi) - \frac{\xi}{2} K_{\nu-1/2}(\xi)\right]. \tag{2.32}$$

Equation (2.31) is also valid for R_{22}, if we set $r_\perp^2 = r_1^2 + r_3^2$. Calculation of the spectrum $\Theta_{22}(\kappa_1, r_2, r_3)$, however, is somewhat more difficult than that of Θ_{11}, because now $r_\perp$ depends on the variable of integration in the Fourier transform, r_1. It turns out that we can use the recurrence relation (eq (2.24)) to put the correlation function in a form that is more conveniently integrated:

$$R_{22}(r_1, r_2, r_3) = \frac{\sigma^2}{2^{\nu-1}\Gamma(\nu)} \left(\frac{r}{\ell}\right)^{\nu} \left[(\nu+1)K_\nu - \frac{1}{2}\left(\frac{r}{\ell}\right) K_{\nu+1} + \frac{r_2^2}{2\ell^2}\left(\frac{r}{\ell}\right)^{-1} K_{\nu-1}\right]. \tag{2.33}$$

Each of the terms in square brackets now is readily transformed with Gradshteyn and Rhyzhik's equation (6.726.4), with the result

$$\Theta_{22}(\kappa_1; r_2, r_3) = \frac{\sigma^2 \ell}{\sqrt{\pi} 2^{\nu-1/2}\Gamma(\nu)} \left(\frac{\xi}{1+\kappa_1^2\ell^2}\right)^{\nu+1/2} \times$$
$$\left[(\nu+1)K_{\nu+1/2}(\xi) - \frac{\xi}{2(1+\kappa_1^2\ell^2)} K_{\nu+3/2}(\xi) + \frac{r_2^2(1+\kappa_1^2\ell^2)}{2\xi\ell^2} K_{\nu-1/2}(\xi)\right]. \tag{2.34}$$

Because of isotropy, $\Theta_{33}(\kappa_1, r_2, r_3)$ must also be given by equation (2.34), except with the indices 2 and 3 interchanged.

The correlation function R_{12} follows from equation (2.26) and the recurrence relation (eq 2.24)):

$$R_{12}(r_1, r_2, r_3) = \frac{\sigma^2}{2\nu\Gamma(\nu)} \left(\frac{r}{\ell}\right)^{\nu-1} \frac{r_1 r_2}{\ell^2} K_{\nu-1}. \tag{2.35}$$

The Fourier transform with respect to r_1 can be determined with the help of Gradshteyn and Rhyzhik's equation (6.726.3), the result being

$$\Theta_{12}(\kappa_1; r_2, r_3) = \frac{\sigma^2 r_2 \kappa_1 \ell}{\sqrt{\pi} 2^{\nu-1/2}\Gamma(\nu)} \left(\frac{\xi}{1+\kappa_1^2\ell^2}\right)^{\nu+1/2} K_{\nu+1/2}(\xi). \tag{2.36}$$

The cross spectrum Θ_{13} is identical to Θ_{12}, except that r_2 in the equation above is replaced by r_3.

The correlation function R_{23} is the same as R_{12}, except with r_3 replacing r_1. Taking the Fourier transform and using Gradshteyn and Rhyzhik's equation (6.726.4), one finds

$$\Theta_{23}(\kappa_1; r_2, r_3) = \frac{\sigma^2 r_2 r_3}{\sqrt{\pi} 2^{\nu-1/2}\Gamma(\nu)\ell} \left(\frac{\xi}{1+\kappa_1^2\ell^2}\right)^{\nu-1/2} K_{\nu-1/2}(\xi)\,. \tag{2.37}$$

When dealing with spectra, it is important to keep clear the distinction between their *one-* and *two-sided* versions (Bendat and Piersol, 1986). The functions Θ_{ij} discussed above are two-sided spectra, being defined for both positive and negative κ_1. In fact, $\Theta_{ij}(-\kappa_1, 0, z, z) = \Theta_{ji}(\kappa_1, 0, z, z)$. Experimentalists more commonly measure one-sided spectra $F_{\alpha\alpha}$, which are defined as zero for negative κ_1 and *twice* $\Theta_{\alpha\alpha}$ for positive κ_1. Note that the variance is recovered by integration of the two-sided spectral density from $\kappa_1 = -\infty$ to $+\infty$, whereas the variance is recovered from the one-sided version by integration from 0 to $+\infty$.

2.6 Two-Dimensional Cross Spectra

We can find the 2D cross spectra by calculating either forward Fourier transforms of the 1D cross spectra, or inverse transforms of the 3D spectra. It is somewhat easier to use the latter approach. Solutions to the necessary integrals can be found in Gradshteyn and Rhyzhik (1994), equations (3.771.2) and (3.771.5). We find

$$\begin{aligned}\phi_{11}(\kappa_1, \kappa_2; r_3) = {} & \frac{\sigma^2\ell^2\zeta_h^{\nu+1}}{\pi 2\nu\Gamma(\nu)(1+\kappa_h^2\ell^2)^{\nu+1}} \\ & \times \left[\left(\nu+\frac{3}{2}\right) K_{\nu+1}(\zeta_h) - \frac{\zeta_h(1+\kappa_1^2\ell^2)}{2(1+\kappa_h^2\ell^2)} K_{\nu+2}(\zeta_h)\right],\end{aligned} \tag{2.38}$$

$$\phi_{33}(\kappa_1, \kappa_2; r_3) = \frac{\sigma^2\kappa_h^2\ell^4\zeta_h^{\nu+2}}{\pi 2^{\nu+1}\Gamma(\nu)(1+\kappa_h^2\ell^2)^{\nu+2}} K_{\nu+2}(\zeta_h)\,, \tag{2.39}$$

$$\phi_{12}(\kappa_1, \kappa_2; r_3) = -\frac{\sigma^2\kappa_1\kappa_2\ell^4\zeta_h^{\nu+2}}{\pi 2^{\nu+1}\Gamma(\nu)(1+\kappa_h^2\ell^2)^{\nu+2}} K_{\nu+2}(\zeta_h)\,, \tag{2.40}$$

$$\phi_{13}(\kappa_1, \kappa_2; r_3) = -\frac{i\sigma^2\kappa_1\ell^3\zeta_h^{\nu+2}}{\pi 2^{\nu+1}\Gamma(\nu)(1+\kappa_h^2\ell^2)^{\nu+3/2}} K_{\nu+1}(\zeta_h)\,, \tag{2.41}$$

where $\zeta_h = (r_3/\ell)\sqrt{1+\kappa_h^2\ell^2}$. The remaining spectra follow from horizontal isotropy:

$$\phi_{22}(\kappa_2, \kappa_1; r_3) = \phi_{11}(\kappa_1, \kappa_2; r_3),$$

and

$$\phi_{23}(\kappa_2, \kappa_1; r_3) = \phi_{13}(\kappa_1, \kappa_2; r_3).$$

Frequently we are most interested in the special case of 2D spectra having no vertical separation. To evaluate this limit, we can use the expansion of the Bessel function for small ξ, equation (2.19). Substituting the expansion into equations (2.38) to (2.41), we find

$$\phi_{11}(\kappa_1, \kappa_2; 0) = \frac{\nu\sigma^2\ell^2}{\pi(1+\kappa_h^2\ell^2)^{\nu+1}}\left[\frac{1}{2} + (\nu+1)\frac{\kappa_2^2\ell^2}{1+\kappa_h^2\ell^2}\right], \tag{2.42}$$

$$\phi_{33}(\kappa_1, \kappa_2; 0) = \frac{\nu(\nu+1)\sigma^2\kappa_h^2\ell^4}{\pi(1+\kappa_h^2\ell^2)^{\nu+2}}, \tag{2.43}$$

$$\phi_{12}(\kappa_1, \kappa_2; 0) = -\frac{\nu(\nu+1)\sigma^2\kappa_1\kappa_2\ell^4}{\pi(1+\kappa_h^2\ell^2)^{\nu+2}}, \tag{2.44}$$

$$\phi_{13}(\kappa_1, \kappa_2; 0) = 0. \tag{2.45}$$

In deriving equations (2.42) to (2.45), use was made of the relationship $\Gamma(\nu+1) = \nu\Gamma(\nu)$.

3. Inhomogeneous CBL Model

All classes of spectra and correlation functions for homogeneous, isotropic turbulence were derived in the previous section. In this section, I introduce the complication of a solid, free slip boundary at $z = 0$. The main effect is to *block* the large eddies, forcing their vertical velocity to zero at the boundary. This introduces vertical inhomogeneity into the correlations and spectra.

3.1 Modification of Two-Dimensional Cross Spectra Near a Boundary

Let us decompose the turbulent velocity fluctuations u_i into contributions from the homogeneous flow (H), such as would exist in the absence of the boundary, and a contribution from blocking at the boundary (B):

$$u_i(x,y,z) = u_i^{(H)}(x,y,z) + u_i^{(B)}(x,y,z). \tag{3.1}$$

Since u_3 must vanish at the boundary, this solution is subject to the condition

$$u_3^{(H)}(x,y,0) + u_3^{(B)}(x,y,0) = 0. \tag{3.2}$$

Because I am not considering mean shear, and viscous effects are negligible for the high Reynolds numbers characteristic of the atmosphere, the boundary does not modify the vorticity field (Hunt and Graham, 1978). Hence, the boundary contribution to the velocity field can be modeled by irrotational, inviscid flow theory, and we can define a velocity potential Φ such that

$$u_i^{(B)} = \nabla\Phi, \tag{3.3}$$

where Φ satisfies Laplace's equation:

$$\nabla^2\Phi = 0. \tag{3.4}$$

Taking the 2D Fourier transform of equation (3.4), we have

$$\left(-\kappa_h^2 + \frac{\partial^2}{\partial z^2}\right)\hat{\Phi}(\kappa_1,\kappa_2,z) = 0, \tag{3.5}$$

where $\kappa_h^2 = \kappa_1^2 + \kappa_2^2$, and the "hat" indicates the 2D Fourier transform. The solution to this equation, subject to the condition that the influence of the boundary becomes negligible as $z \to \infty$, is

$$\hat{\Phi} = A\exp(-\kappa_h z). \tag{3.6}$$

From the boundary condition (eq (3.2)),

$$A = \hat{u}_3^{(H)}(\kappa_1,\kappa_2,0)/\kappa_h. \tag{3.7}$$

By Fourier transforming equation (3.3), we can now easily show that

$$\hat{u}_i^{(B)}(\kappa_1,\kappa_2,z) = m_i(\kappa_1,\kappa_2)\exp(-\kappa_h z)\hat{u}_3^{(H)}(\kappa_1,\kappa_2,0), \tag{3.8}$$

in which

$$m_i(\kappa_1,\kappa_2) = (i\kappa_1/\kappa_h, i\kappa_2/\kappa_h, -1). \tag{3.9}$$

We have now determined the effect of the boundary by solving for $\hat{u}_i^{(B)}$ in terms of $\hat{u}_i^{(H)}$. In principle, this allows us to determine all the correlations and spectra. The 2D cross spectra are equal to

$$\phi_{ij}(\kappa_1,\kappa_2,z,z') = \langle \hat{u}_i(\kappa_1,\kappa_2,z)\hat{u}_j^*(\kappa_1,\kappa_2,z')\rangle. \tag{3.10}$$

Since, from equations (3.1) and (3.8),

$$\hat{u}_i(\kappa_1,\kappa_2,z) = \hat{u}_i^{(H)}(\kappa_1,\kappa_2,z) + m_i\exp(-\kappa_h z)\hat{u}_3^{(H)}(\kappa_1,\kappa_2,0), \tag{3.11}$$

we have the result

$$\begin{aligned}\phi_{ij}(\kappa_1,\kappa_2;z,z') = {} & \phi_{ij}^{(H)}(\kappa_1,\kappa_2;z'-z) \\ & + e^{-\kappa_h z'} m_j(\kappa_1,\kappa_2)\phi_{3i}^{(H)*}(\kappa_1,\kappa_2;z) \\ & + e^{-\kappa_h z} m_i^*(\kappa_1,\kappa_2)\phi_{3j}^{(H)}(\kappa_1,\kappa_2;z') \\ & + e^{-\kappa_h(z+z')} m_i^*(\kappa_1,\kappa_2)m_j(\kappa_1,\kappa_2)\phi_{33}^{(H)}(\kappa_1,\kappa_2;0).\end{aligned} \tag{3.12}$$

The second term on the right was simplified by

$$\phi_{ij}^{(H)}(\kappa_1,\kappa_2;-z) = \phi_{ji}^{(H)*}(\kappa_1,\kappa_2;z), \tag{3.13}$$

which can be proven from the Fourier transform definition.

Equation (3.12) is the basis for the rest of the work in this report. (With some work, one can show its equivalence to equation (2.50) in Hunt and Graham (1978); this is demonstrated in app B.) Its main utility is that it gives the vertically inhomogeneous, boundary-influenced cross spectra ϕ_{ij} entirely in terms of the homogeneous cross spectra $\phi_{ij}^{(H)}$, which were given in section 2.6. For example, the autospectrum ($i = j$, $z = z'$) for a component of the horizontal velocity is

$$\begin{aligned}\phi_{11}(\kappa_1,\kappa_2;z,z) = {} & \phi_{11}^{(H)}(\kappa_1,\kappa_2;0) - \frac{2i\kappa_1}{\kappa_h}e^{-\kappa_h z}\phi_{13}^{(H)}(\kappa_1,\kappa_2;z) \\ & + \left(\frac{\kappa_1}{\kappa_h}\right)^2 e^{-2\kappa_h z}\phi_{33}^{(H)}(\kappa_1,\kappa_2;0).\end{aligned} \tag{3.14}$$

(In deriving this result, use was made of the fact that $\phi_{13}^{(H)}$ is purely imaginary; see sect. 2.6.) For the vertical velocity autospectrum, we have

$$\phi_{33}(\kappa_1,\kappa_2;z,z)=\left(1+e^{-2\kappa_h z}\right)\phi_{33}^{(H)}(\kappa_1,\kappa_2;0)-2e^{-\kappa_h z}\phi_{33}^{(H)}(\kappa_1,\kappa_2;z). \tag{3.15}$$

Equation (3.15) is the same as equation (2.12a) in Hunt (1984), after one performs the integration over κ_2 in Hunt's equation.

The first term in equation (3.12) is the spectrum that would be observed if there were no boundary effects. The remaining terms decay exponentially with increasing height and decreasing horizontal eddy scale.

3.2 Modification of One-Dimensional Correlations and Cross Spectra Near a Boundary

Unlike the homogeneous case, in general it is not possible to find correlation functions or 1D cross spectra from ϕ_{ij} analytically. One must compute the Fourier transform or integration numerically. For example, the 1D cross spectra in the x-direction are given by

$$\Theta_{ij}(\kappa_1;0,z,z')=\int_{-\infty}^{\infty}\phi_{ij}(\kappa_1,\kappa_2;z,z')\,d\kappa_2. \tag{3.16}$$

We can find the 1D correlation function $R_{ij}(r,0,0)$ by numerically calculating the inverse Fourier transform of $\Theta_{ij}(\kappa,0,0)$. This is not difficult with a fast Fourier transform (FFT).

Some example results are shown in figures 4 and 5. The calculations are for three cases: $z=z'=0.01\ell$, $z=z'=0.1\ell$, and the limiting homogeneous case ($z=z'\to\infty$). The most obvious feature of the correlations and spectra is that the vertical velocity is severely attenuated near the boundary, by a loss of long-wavelength (low-wavenumber) energy.

Another interesting feature is that $R_{11}(r,0;z,z)\approx R_{22}(r,0;z,z)$ near the boundary (and hence also $\Theta_{11}(\kappa;0,z,z)\approx\Theta_{22}(\kappa;0,z,z)$). Note that this is *not* the case away from the boundary. Let us consider the behavior of the horizontal velocity spectra at small heights in more detail. Making the approximations $z/\ell\ll 1$ and $\kappa_h z\ll 1$ in equation (2.38), we find

$$\phi_{11}(\kappa_1,\kappa_2;0)\approx\frac{\nu\sigma^2\ell^2}{\pi(1+\kappa_h^2\ell^2)^{\nu+1}}\left[\frac{1}{2}+(\nu+1)\frac{\kappa_h^2\ell^2}{1+\kappa_h^2\ell^2}\right]. \tag{3.17}$$

This is the same as equation (2.42), except that the occurrence of κ_2 in the second term in the square brackets has been replaced by κ_h. Since ϕ_{11} depends only on κ_h near the ground, so too must ϕ_{22}, by horizontal isotropy. Hence, when the 2D spectra are integrated, we find $\Theta_{11}\approx\Theta_{22}$.

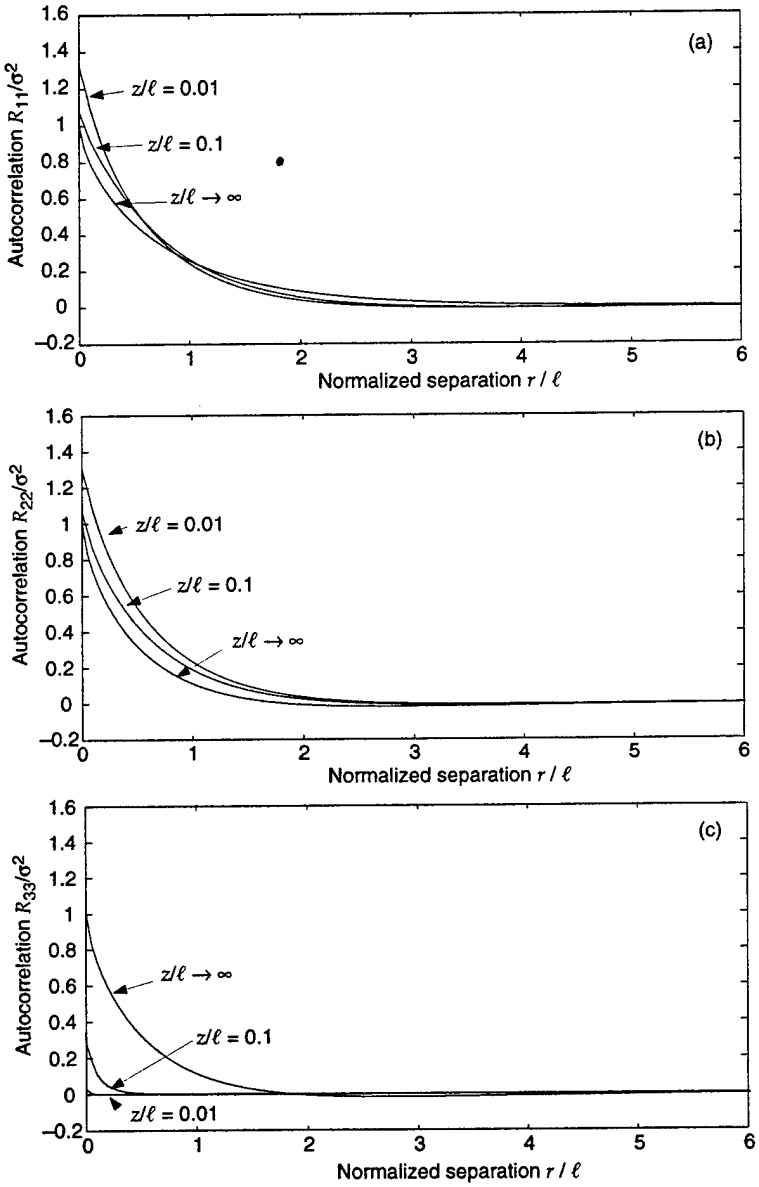

Figure 4: Inhomogeneous, autocorrelation function with displacement r along x_1 axis. (a) $i = 1$ velocity component. (b) $i = 2$. (c) $i = 3$.

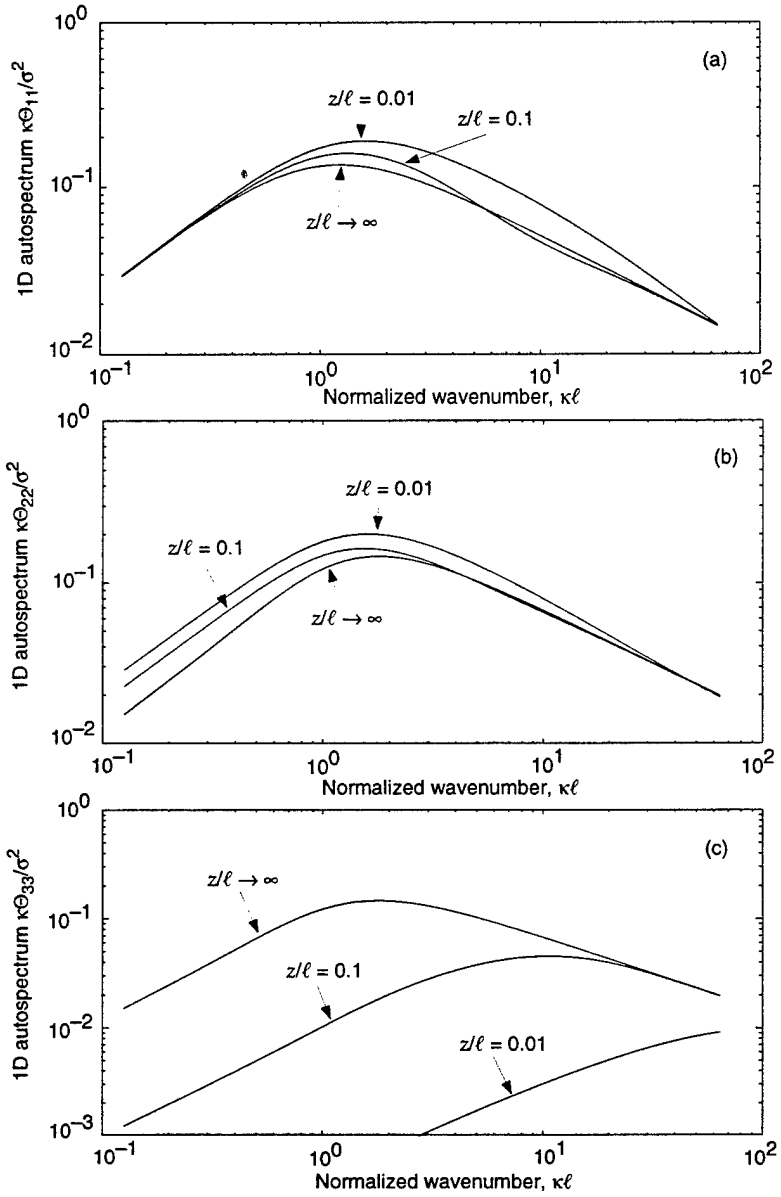

Figure 5: Inhomogeneous, autospectral function, as a function of wavenumber along κ_1 axis. (a) $i = 1$ velocity component. (b) $i = 2$. (c) $i = 3$.

3.3 Parameter Selection

Besides ν, which is normally set to 1/3, the only two adjustable parameters in the correlation/spectral model are the variance σ^2 and the length scale ℓ. We need to select values for these parameters that are appropriate for a CBL. Caughey and Palmer (1979) found the variance of all three velocity components, away from the influence of the ground, to be

$$\sigma^2 = 0.35 w_*^2, \tag{3.18}$$

where $w_* = (Qgz_i/T_0)^{1/3}$ is the CBL velocity scale, with Q being the surface heat flux, g the gravitational acceleration, z_i the inversion height, and T_0 the surface temperature.

The length scale ℓ can be chosen in a variety of ways. I follow Peltier *et al.* (1996) by choosing it to match the inertial subrange asymptote. In the inertial subrange, we must have

$$\hat{f}(\kappa) = (\alpha_1/2)\epsilon^{2/3}\kappa^{-5/3}, \tag{3.19}$$

where $\hat{f}(\kappa)$ is the 1D longitudinal spectrum, ϵ the TKE dissipation rate, and α_1 is a constant, approximately equal to 0.52 (Kaimal *et al.* 1972). (The coefficient in equation (3.19) is $\alpha_1/2$, rather than α_1 as in Kaimal *et al.* (1972), because $\hat{f}(\kappa)$ is a two-sided spectrum, whereas Kaimal *et al.* dealt with a one-sided spectrum. This distinction is discussed at the end of sect. 2.5.) Taking the high wavenumber limit of equation (2.17) and comparing it with equation (3.19), we have the requirement

$$\ell = \left[\frac{2\Gamma(5/6)}{\sqrt{\pi}\Gamma(1/3)\alpha_1}\right]^{3/2} \frac{\sigma^3}{\epsilon}. \tag{3.20}$$

For freely convective conditions, $\epsilon \approx 0.8 w_*^3/z_i$ (Caughey and Palmer, 1979). Hence, equations (3.18) and (3.20) together imply

$$\ell = 0.23 z_i. \tag{3.21}$$

4. Comparisons With Previous Results

This section compares the model developed above with field measurements, large-eddy simulation (LES) data, and other models of CBL structure. Because $\phi_{ij}(\kappa_1, \kappa_2; z, z')$ is not easily determined directly from field measurements, the comparisons I make are for a variety of limiting cases, chosen to represent a variety of vertical and horizontal structural characteristics and a broad range of spectral scales.

4.1 Energy Spectra

Peltier *et al.* (1996) recently developed a model for horizontal spectra in the atmospheric boundary layer. Their model, which included the surface blocking effect on large eddies, agreed quite well with measured spectra for both the horizontal and vertical velocities.

Peltier *et al.* developed equations for the TKE of the horizontal and vertical velocities, defined in my notation as

$$E_h(\kappa_h; z) = \pi\kappa_h \left[\phi_{11}(\kappa_1, \kappa_2; z, z) + \phi_{22}(\kappa_1, \kappa_2; z, z) \right], \tag{4.1}$$

and

$$E_v(\kappa_h; z) = \pi\kappa_h \phi_{33}(\kappa_1, \kappa_2; z, z). \tag{4.2}$$

Their model for E_h was

$$E_h^p(\kappa_h) = \frac{c_1 \ell_1^2 s^2 \kappa_h}{[c_2 + (\kappa_h \ell_1)^2]^{4/3}} = \frac{c_p \kappa_h \ell_p^2}{(1 + \kappa_h^2 \ell_p^2)^{4/3}}, \tag{4.3}$$

where, in the second version, I have simplified the equation using the substitutions $\ell_p = \ell_1/\sqrt{c_2}$ and $c_p = c_1 s^2 / c_2^{1/3}$. The superscript p indicates the Peltier *et al.* model. The vertical TKE spectrum is related to the horizontal spectrum by a transfer function $T(\kappa_h, z)$:

$$E_v^p(\kappa_h) = T(\kappa_h, z) E_h^p(\kappa_h). \tag{4.4}$$

The transfer function is tailored "to meet the continuity constraint [at the lower boundary] and to maintain the proper level in the inertial subrange." Peltier *et al.* select the constants and the transfer function such that

$$E_h^P(\kappa_h; z) = \frac{0.85 \kappa_h z_i^2}{[23 + (\kappa_h z_i)^2]^{4/3}} w_*^2, \tag{4.5}$$

and

$$T(\kappa_h; z) = \frac{(\kappa_h z)^2/2}{0.62 + \frac{7}{8}(\kappa_h z)^2}. \tag{4.6}$$

The equations for E_h and E_v corresponding to this report's model follow from equations (3.14) and (3.15), after the appropriate spectral forms are substituted from section 2.6. The results are

$$E_h(\kappa_h; z) = \frac{\sigma^2 \kappa_h \ell^2}{(1+\kappa_h^2\ell^2)^{\nu+1}} \left[\nu + \frac{\nu(\nu+1)\kappa_h^2\ell^2}{1+\kappa_h^2\ell^2} \left(1 + e^{-2\kappa_h z}\right) - \frac{\kappa_h \ell \zeta_h^{\nu+2}}{2^\nu \Gamma(\nu)\sqrt{1+\kappa_h^2\ell^2}} e^{-\kappa_h z} K_{\nu+1}(\zeta_h) \right], \tag{4.7}$$

and

$$E_v(\kappa_h; z) = \frac{\sigma^2 \kappa_h^3 \ell^4}{(1+\kappa_h^2\ell^2)^{\nu+2}} \left[\nu(\nu+1) \left(1 + e^{-2\kappa_h z}\right) - \frac{\zeta_h^{\nu+2}}{2^\nu \Gamma(\nu)} e^{-\kappa_h z} K_{\nu+2}(\zeta_h) \right]. \tag{4.8}$$

The two models are compared in figure 6, for $z = 10$ m and $z_i = 1000$ m. The differences between the models are quite small, well within the scatter of the field measurements plotted in Peltier *et al.* (1996). Both models predict strong damping of large-scale (small $\kappa_h z_i$) vertical velocity structure near the surface.

4.2 Variances

By setting $r_1 = r_2 = 0$ in equation (2.4), one has

$$R_{ij}(0, 0, z, z') = \int_{-\infty}^{\infty} \int_{-\infty}^{\infty} \phi_{ij}(\kappa_1, \kappa_2; z, z')\, d\kappa_1\, d\kappa_2. \tag{4.9}$$

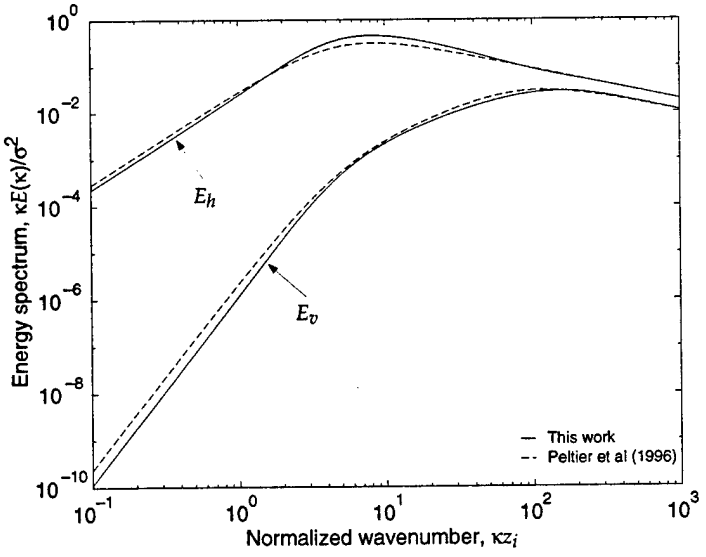

Figure 6: Comparison of energy spectral models from Peltier *et al.* (1996) and this work. A height of $z =$ 10calculations.

The height-dependent (co)variances are defined as

$$\sigma_{ij}^2(z) = R_{ij}(0,0,z,z). \tag{4.10}$$

In general, we must perform the 2D integration in equation (4.9) numerically. Alternatively, we can integrate the energy spectra in one dimension, e.g.,

$$\sigma_{33}^2(z) = 2\int_0^\infty E_v(\kappa_h; z)\, d\kappa_h. \tag{4.11}$$

Model predictions for the variances are plotted in figure 7, and compared to data from Caughey and Palmer (1979) and an LES of a highly convective CBL. Caughey and Palmer's data are a combined set from the Minnesota and Ashchurch experiments. The LES data were supplied by S. Khanna and J. Brasseur of the Pennsylvania State University. Their code was based on Moeng's (1984), and the computational grid for the run was 5 km on a side in the horizontal and 2 km in the vertical, with 128^3 grid points. The surface heat flux was 0.24 K-m/s, and the geostrophic wind speed was 1 m/s. The resulting value for $-z_i/L$ (where L is the Monin-Obukhov length) was 730.

Although there is much scatter to the field data, there is generally good agreement with the model predictions. In particular, the near-surface height dependence of the vertical velocity variance is predicted extremely well. The variances for the LES data tend to be higher than either the predictions or field data, by roughly 25 percent.

Let us analyze the near-surface height dependence of $\sigma_{33}^2(z)$ in detail. When $z \ll \ell$, most of the spectral contribution to $\sigma_{33}^2(z)$ comes from wavenumbers

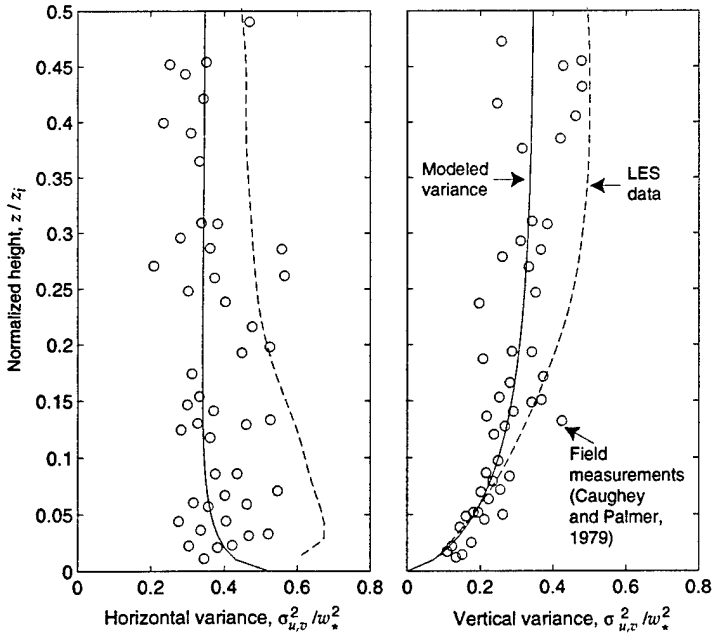

Figure 7: Velocity variances as a function of height.

such that $\kappa_h z \ll 1$. Hence, in equation (3.15), we can make the approximation $\exp(-\kappa_h z) \approx 1$, resulting in

$$\phi_{33}(\kappa_1, \kappa_2; z, z) = 2\phi_{33}^{(H)}(\kappa_1, \kappa_2; 0) - 2\phi_{33}^{(H)}(\kappa_1, \kappa_2; z). \tag{4.12}$$

Taking the Fourier transform, and setting $r_1 = r_2 = 0$, we have

$$\sigma_{33}^2(z) = 2\sigma^2 - 2R_{33}^{(H)}(0, 0, z). \tag{4.13}$$

The function $R_{33}^{(H)}(0, 0, z)$ is an example of a longitudinal autocorrelation function: the displacement is taken in the same direction as the velocity component. The longitudinal autocorrelation $f(r) = R_{33}^{(H)}(0, 0, r)/\sigma^2$ was given earlier as equation (2.18). Expanding the modified Bessel function for small arguments, we find

$$\sigma_{33}^2(z) \approx \frac{2\sigma^2\Gamma(1-\nu)}{\nu\Gamma(\nu)} \left(\frac{z}{2\ell}\right)^{2\nu}. \tag{4.14}$$

Setting the parameters ν, σ^2, and ℓ as discussed in section 2, we arrive at

$$\sigma_{33}^2(z) \approx 1.8 w_*^2 \left(\frac{z}{z_i}\right)^{2/3}. \tag{4.15}$$

This result is identical to Caughey and Palmer's (1979) equation 3. Since $w_{fc}/w_* = (z/z_i)^{1/3}$ (where w_{fc} is the local free convection velocity scale), the result agrees with previous findings that the vertical velocity obeys local free convective scaling near the surface (Wyngaard, Coté, and Izumi, 1971). In the model in this report, the free convective scaling has appeared as a natural consequence of the 3D correlation/spectral model.

4.3 Vertical Velocity Correlations

In this section, I consider correlations of the vertical velocity at two different heights, $R_{33}(0, 0, z, z')$. This function can be evaluated from equation (4.9). It is convenient to convert the correlation function to a correlation coefficient, by normalizing by the variance at each height:

$$\rho_{33}(z, z') = \frac{R_{33}(0, 0, z, z')}{\sigma_{33}(z)\sigma_{33}(z')}. \tag{4.16}$$

Hunt *et al.* (1988) considered models for $\rho_{33}(z, z')$. Based on a heuristic argument involving image eddies, they concluded that

$$\rho_{33}(z, z') \approx \frac{z}{z'}, \tag{4.17}$$

for $z \ll z' \ll z_i$. Hunt *et al.* found that this simple equation agrees quite well with experimental data, as shown in figure 8. Also shown on the plot are predictions from the present report's model for several values of z'/z_i. There is good agreement when z' is less than about $0.1 z_i$, but as z' is increased, the models diverge. This is not particularly surprising, since Hunt *et al.*'s equation strictly applies only for small z'/z_i. Hunt *et al.*'s experimental data cover a range of z/z_i values from about 0.01 and 0.32. Most of their data points for small z/z' correspond to relatively large values for z'/z_i.

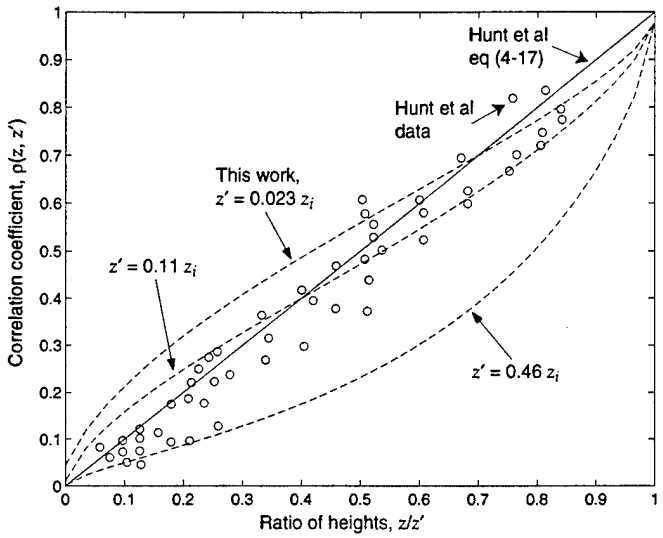

Figure 8: Correlation coefficient for vertical velocity, $\rho_{33}(z, z')$: solid line represents Hunt *et al.*'s (1988) equation. Present model is represented by dashed lines, for which three values of z' are shown.

4.4 One-Dimensional Spectra

Longitudinal autospectra $\Theta_{\alpha\alpha}(\kappa_1; 0, z, z')$, for each of the three velocity components, are plotted in figure 9 and compared to data from the Minnesota experiment (Kaimal, 1978). The 1D spectra were determined numerically by integration of 2D spectra. Predictions are shown for two heights, $z = 4$ and $z = 32$ m, as Kaimal's measurements included data taken from various heights between these limiting values. The inversion height was taken as $z_i = 1000$ m for the predictions. (When the predictions are normalized as in figure 9, they are not very sensitive to the value of z_i.) The spectra for the horizontal velocity components are normalized by the variance, which is height dependent. The vertical velocity spectrum is normalized by $u_*^2 \phi_\epsilon^{2/3} / \kappa_1$, where $\phi_\epsilon^{2/3} \approx 0.75 |z/L|^{2/3}$ for convective conditions (Kaimal, 1978).

Agreement between the measured spectra and the predictions is fairly good. For the horizontal velocities, there is more high-frequency energy in the measurements; shear-generated turbulence is the likely cause. The cross-wind component of the horizontal velocity (Θ_{22}) has slightly more low-frequency energy than the predictions. For the vertical velocity, the spectral peak in the prediction tends to be sharper than the data.

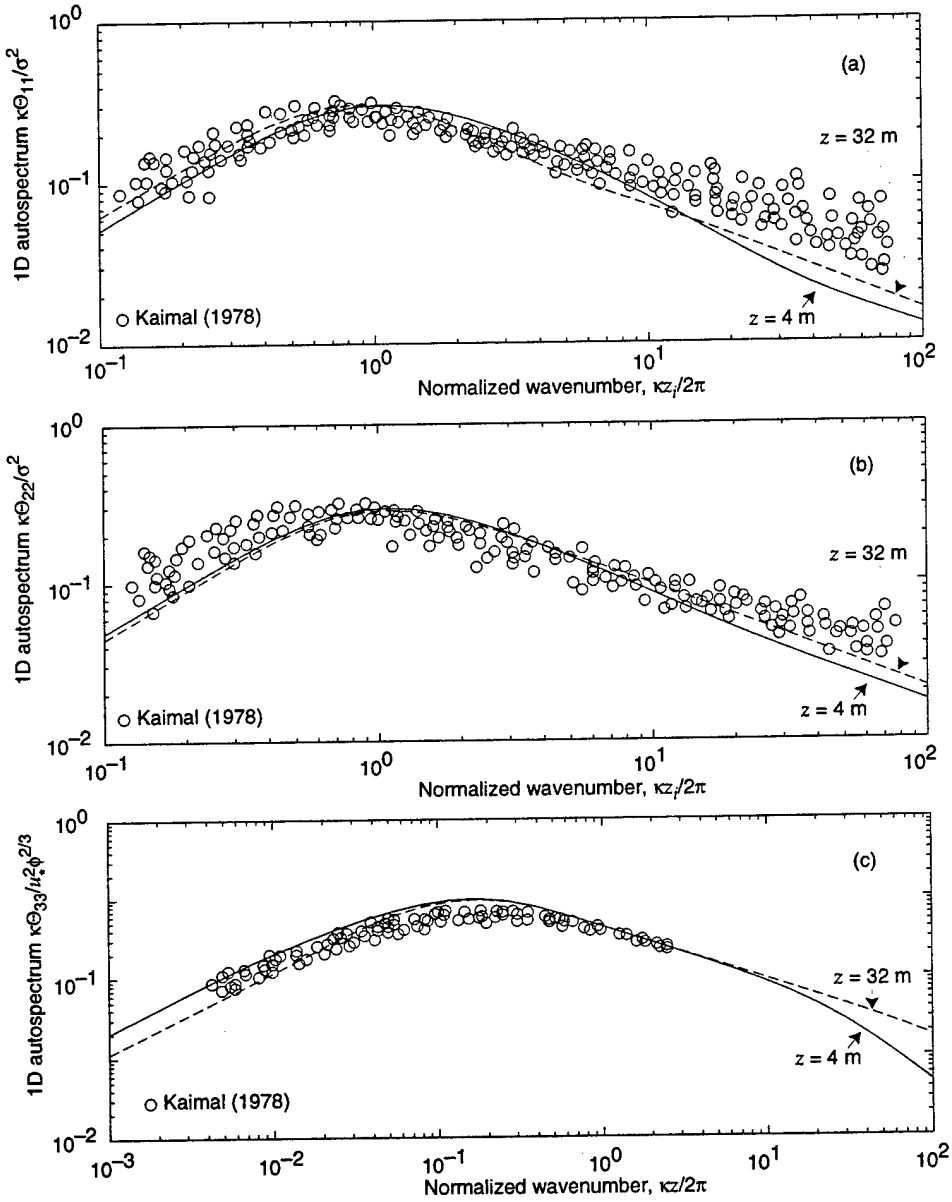

Figure 9: One-dimensional, longitudinal spectral densities: (a) u-component; (b) v-component; (c) w-component.

4.5 Vertical Cross Coherence

The vertical cross coherence for the u_1 velocity component is defined as

$$\mathrm{Coh}_{11}(\kappa_1) = \frac{\Theta_{11}^2(\kappa_1, 0, z, z')}{\Theta_{11}(\kappa_1, 0, z, z)\Theta_{11}(\kappa_1, 0, z', z')}. \tag{4.18}$$

Cross coherences such as equation (4.18) often have been modeled in the literature by the use of *Davenport similarity* (Davenport, 1961). Davenport's two hypotheses are (1) the coherence depends only on $\Delta n = f\Delta z/V = \kappa_1 \Delta z/2\pi$, where $\Delta z = z' - z$; and (2) the dependence on Δn is approximately exponential, $\mathrm{Coh}(\kappa_1) = \exp(-a\Delta n)$, where a is a constant or depends in a simple manner on height, stability, etc (Soucy, Woodward, and Panofsky, 1982). In this section, I ascertain the extent to which the spectral model discussed in this report satisfies Davenport similarity, and also compare it to experimental measurements of the vertical cross coherence.

We compute the coherence Coh_{11} by integrating the 2D cross spectrum, as in equation (3.16). Plots are shown in figure 10. For comparison, I also plot experimental data recorded at White Sands Missile Range, NM (Panofsky and Dutton, 1984), and the Davenport exponential model, $\exp(-a\Delta n)$ with $a = 10$. The value $a \approx 10$ is thought to be representative of moderately convective conditions (Soucy, Woodward, and Panofsky, 1982). Both the spectral model and the Davenport model agree fairly well with the data. There is a trend in the data for greater coherence at large Δn than is predicted by the spectral model.

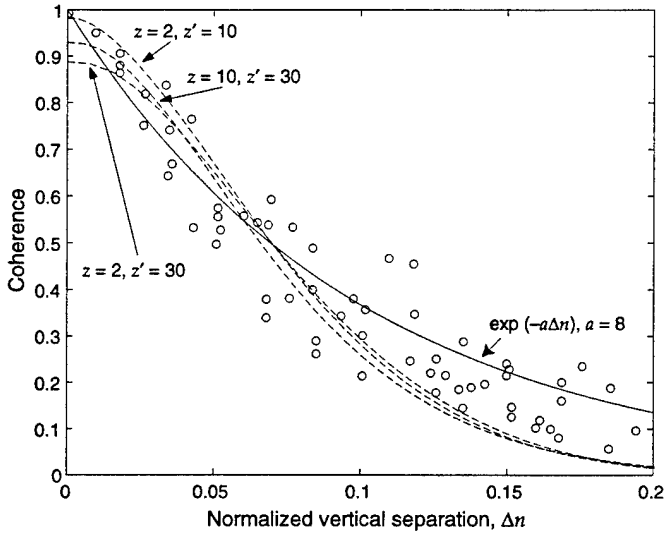

Figure 10: Vertical coherence of longitudinal velocity, as a function of $\Delta n = \kappa_1 \Delta z/2\pi$. Model predictions are shown for three different combinations of z and z'.

4.6 Integral Length Scales

The integral length scale in the x_1 direction is defined as

$$L_{ij,1}(z) = \frac{1}{\sigma_{ij}^2(z)} \int_0^\infty R_{ij}(r_1, 0; z, z)\, dr_1, \tag{4.19}$$

and similarly for $L_{ij,2}(z)$. By Fourier transforming equation (2.6) with respect to κ_2, and then evaluating the result at $\kappa_1 = 0$, $r_2 = 0$, one can show

$$L_{ij,1}(z) = \frac{\pi}{\sigma_{ij}^2(z)} \int_{-\infty}^\infty \phi_{ij}(0, \kappa_2; z, z)\, d\kappa_2. \tag{4.20}$$

Let us take a moment to consider the limiting values for the length scales far from the ground's influence ($z \gg \ell$) and close to the ground ($z \ll \ell$). In the former case, we can use the spectra developed for homogeneous, isotropic turbulence. It can be shown, by integrating equation (2.42), that

$$L_{11,1}^{(H)} = \frac{\sqrt{\pi}\Gamma(\nu + 1/2)}{\Gamma(\nu)} \ell = 0.747\ell \approx 0.17 z_i. \tag{4.21}$$

Furthermore, since $\phi_{22}^{(H)}(0, \kappa_1; 0) = \phi_{11}^{(H)}(\kappa_1, 0; 0)$ by isotropy, integration yields

$$L_{22,1}^{(H)} = \frac{\sqrt{\pi}\Gamma(\nu + 1/2)}{2\Gamma(\nu)} \ell = 0.373\ell \approx 0.086 z_i. \tag{4.22}$$

The quantity $L_{11,1}^{(H)}$ is an example of a *parallel* length scale $L_\parallel$, in which the spatial integration is performed in the same direction as the velocity axis. On the other hand, $L_{22,1}^{(H)}$ is a *perpendicular* length scale $L_\perp$, since the integration is normal to the velocity axis. $L_{33,1}^{(H)}$, of course, is also a perpendicular scale. In homogeneous, isotropic turbulence, $L_\parallel = 2L_\perp$ (Batchelor, 1953).

At the ground level, on the other hand, it can be shown from equation (3.17) that

$$L_{11,1}(0) = L_{22,1}(0) = \frac{2\sqrt{\pi}\Gamma(\nu + 1/2)}{3\Gamma(\nu)} \ell = 0.498\ell \approx 0.11 z_i. \tag{4.23}$$

It is interesting that near the ground, the parallel and perpendicular length scales become equal, and are equal to two-thirds times the free-space parallel scale. The length scale for the vertical velocity vanishes at ground level, as is evident from equation (3.15).

Model predictions, field data, and LES data for the integral length scales are compared in figure 11. The LES run was described in section 4.2. The field data were recorded during the Air Mass Transformation Experiment (AMTEX), and analyzed by Lenschow and Stankov (1986). Note that Lenschow and Stankov found little azimuthal dependence for the horizontal length scales, and hence combined the data for the two horizontal velocity components.

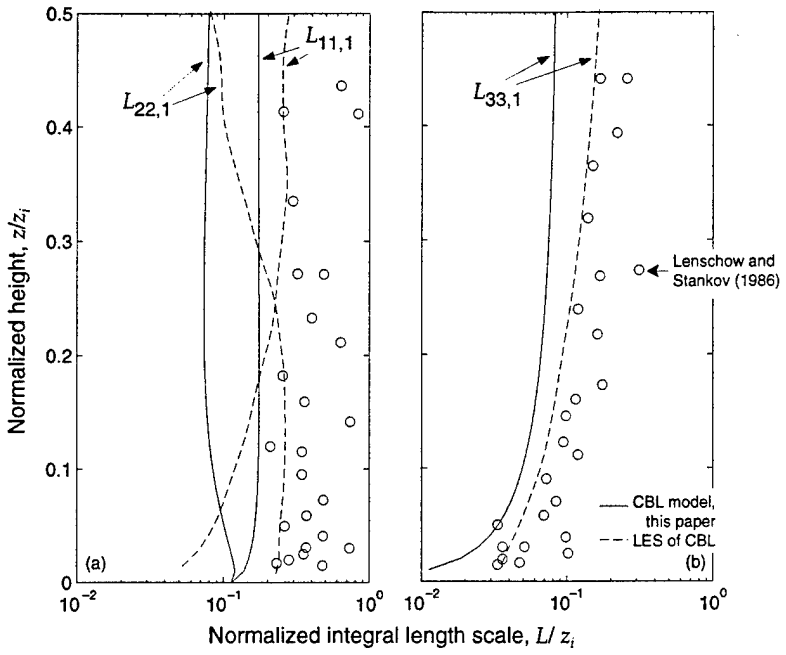

Figure 11: Integral length scales from AMTEX (Lenschow and Stankov, 1986) (circles), an LES of the CBL (dashed lines), and this report's model (solid line). Left: two horizontal velocity components; right: vertical velocity.

On the whole, agreement between the integral length scale predications and the data is somewhat poorer than for the quantities considered in previous sections. In particular, the length scales from AMTEX tend to be several times larger than the model predictions. The LES data generally fall somewhere between. But there is good qualitative agreement, at least, as to the height dependence of the length scales for the different velocity components. The length scale for the vertical velocity $L_{33,1}$ starts out small near the ground and increases with height. The model and LES both have $L_{22,1}$ decreasing with height, although the surface value is about twice as large for the LES. Similarly, both the model and LES have $L_{11,1}$ decreasing with height. However, in the LES results, $L_{11,1}$ nearly vanishes at the surface. This could result from the finite resolution of the LES.

5. Conclusion

A 3D correlation/spectral model for turbulent velocities in the CBL was developed in this report and compared with data for a number of limiting cases, such as variances, vertical correlations, 1D spectra, and integral length scales. In most cases, agreement was quite good. Although previous researchers have developed simpler formulations than the 3D model, which also compare favorably with the data and are valid for some of the individual cases, the 3D model is based on a single, unified approach to CBL statistics. And most importantly, it can be used in situations where complete information on 3D turbulence statistics is required. Future work on the model could include incorporation of scalar fields (e.g., temperature and water vapor) and incorporation of ground roughness effects.

Acknowledgements

This work was begun while the author was a Research Associate at the Pennsylvania State University, Department of Meteorology, sponsored by the Office of Naval Research's Marine Boundary Layer Advanced Research Initiative, Grant N00014-92-J-1688. The author is indebted to J. C. Wyngaard for his valuable suggestions and encouragement. Thanks also to S. Khanna and J. Brasseur for providing the high-resolution LES data.

Appendix A. More on TKE Spectrum and Production

As discussed in the introduction to the main body of this report, the scales of motion in a turbulent flow can be roughly partitioned into three subranges: energy-containing, inertial, and dissipative. The energy-containing range consists of spatial scales λ ($\sim 1/\kappa$) much larger than ℓ (and hence $\kappa \ll 1/\ell$), the inertial subrange of scales smaller than ℓ but larger than η ($1/\ell \ll \kappa \ll 1/\eta$), and the dissipative subrange of scales smaller than η ($\kappa \gg 1/\eta$). The length scale η is called the *Kolmogorov microscale*, and it is equal to $(\nu^3/\epsilon)^{1/4}$, where ν is the kinematic viscosity and ϵ the dissipation rate of turbulent kinetic energy (TKE) (Kolmogorov, 1941).

The TKE model used in this report, equation (2.14), applies only to the energy-containing and inertial subranges. This is not normally a problem in acoustics, unless one is interested in ultrasonic frequencies. But in order to tie up some loose ends and explain how figure 1 was created, I discuss in this appendix how equation (2.14) can be extended to the dissipative subrange.

The starting point is the following equation, due to Corrsin (1964), which is valid only for the inertial and dissipative subranges:

$$E(\kappa) = \alpha\epsilon^{2/3}\kappa^{-5/3}\exp\left[-\frac{3}{2}\alpha(\kappa\eta)^{4/3}\right], \tag{A-1}$$

where α is a constant approximately equal to 1.6. By approximating equation (A-1) to small $\kappa\eta$, equation (2.14) in the body of the report to large $\kappa\ell$, and equating the results, we have the following constraint for the inertial subrange:

$$\alpha\epsilon^{2/3} = \frac{4\Gamma(17/6)}{\sqrt{\pi}\Gamma(1/3)}\sigma^2\ell^{-2/3}. \tag{A-2}$$

Substituting this result into equation (2.14), and combining with (eq A-1), we find

$$E(\kappa) = \alpha(\epsilon\ell)^{2/3}\frac{\kappa^4\ell^5}{(1+\kappa^2\ell^2)^{17/6}}\exp\left[-\frac{3}{2}\alpha(\kappa\eta)^{4/3}\right]. \tag{A-3}$$

This equation should work reasonably well throughout the turbulent spectrum. It is plotted in figure 1(a) in the body of the report for $\ell = 10^4\eta$.

Tennekes and Lumley (1972) show that the flux of TKE through the wavenumber κ is

$$T(\kappa) = \alpha^{-3/2}\kappa^{5/2}E^{3/2}. \tag{A-4}$$

Using equation (A-3), we find

$$T(\kappa) = \epsilon\frac{(\kappa\ell)^{17/2}}{(1+\kappa^2\ell^2)^{17/4}}\exp\left[-\frac{9}{4}\alpha(\kappa\eta)^{4/3}\right]. \tag{A-5}$$

Note that in the inertial subrange, $T(\kappa) = \epsilon$. This is because energy is neither produced nor destroyed in the inertial subrange; it is merely transferred to

smaller scales, eventually being dissipated by viscosity. The *production* of TKE at a given wavenumber is

$$P(\kappa) = \frac{dT(\kappa)}{d\kappa}. \tag{A-6}$$

TKE production using equation (A-5) was plotted in figure 1(b). Note that production is positive in the energy-containing subrange, and negative in the dissipative subrange, as expected. The total area under the curve sums to zero, since the net production of TKE must be zero if conditions are stationary.

Appendix B. Derivation of the Two-Dimensional Cross Spectral Equation From Hunt and Graham's (1978) Result

Hunt and Graham (1978) considered the spectra for free-stream turbulence above a plane boundary. The turbulence was generated by a flow moving through a grid, with the boundary moving at the same speed as the mean flow. Hence, there was no shear generation of turbulence at the boundary, and the only effect of the boundary was to block the flow. This makes Hunt and Graham's spectral model appropriate for the convective boundary layer (CBL), particularly when the turbulence generated by the mean wind is negligible in comparison to convectively generated turbulence. The assumptions that go into the Hunt and Graham model are actually equivalent to those used in this report (sect. 3); mainly, the blocking flow at the boundary is assumed to be irrotational. Hence, Hunt and Graham's final results should be equivalent to ours. The equivalence is demonstrated in this appendix.

Hunt and Graham's equation (2.50), for the one-dimensional (1D), longitudinal cross spectra, is the starting point for this proof. Rewriting that equation so that the coordinate system follows the atmospheric convention (z vertical), we have

$$\begin{aligned}\Theta_{ij}(\kappa_1;\mathbf{x},\mathbf{x}') &= \int_{-\infty}^{\infty}\int_{-\infty}^{\infty} M^*_{i\ell}(x,z;\boldsymbol{\kappa})M_{jm}(x',z';\boldsymbol{\kappa}) \\ &\times \exp[i\kappa_2(y-y')]\Phi^{(H)}_{\ell m}(\boldsymbol{\kappa})\,d\kappa_2\,d\kappa_3. \end{aligned} \tag{B-1}$$

Here $\Phi^{(H)}_{\ell m}$ is the "homogeneous" 3D spectrum: the spectrum generated by the grid that would persist without any blocking from the boundary. The tensor M_{ij} is given by Hunt and Graham as

$$M_{ij}(x,z;\boldsymbol{\kappa}) = \begin{bmatrix} e^{i\kappa_3 z+i\kappa_1 x} & 0 & i(\kappa_1/\kappa_h)e^{-\kappa_h z+i\kappa_1 x} \\ 0 & e^{i\kappa_3 z+i\kappa_1 x} & i(\kappa_2/\kappa_h)e^{-\kappa_h z+i\kappa_1 x} \\ 0 & 0 & (e^{i\kappa_3 z}-e^{-\kappa_h z})e^{i\kappa_1 x} \end{bmatrix} \tag{B-2}$$

where $\kappa_h^2 = \kappa_1^2+\kappa_2^2$. Equivalently, one can write

$$M_{ij}(x,z;\boldsymbol{\kappa}) = e^{i\kappa_1 x}\left(\delta_{ij}e^{i\kappa_3 z} + m_i(\kappa_1,\kappa_2)\delta_{j3}e^{-\kappa_h z}\right), \tag{B-3}$$

with

$$m_i(\kappa_1,\kappa_2) = (i\kappa_1/\kappa_h, i\kappa_2/\kappa_h, -1). \tag{B-4}$$

The 2D cross spectrum ϕ_{ij} follows from Θ_{ij} if we omit the Fourier transformation integral involving κ_2. Doing so, and setting $x=x'$, $y=y'$, we find

$$\phi_{ij}(\kappa_1,\kappa_2;z,z') = \int_{-\infty}^{\infty} M^*_{i\ell}(0,z;\boldsymbol{\kappa})M_{jm}(0,z';\boldsymbol{\kappa})\Phi^{(H)}_{\ell m}(\boldsymbol{\kappa})\,d\kappa_3. \tag{B-5}$$

Substituting with equation (B-3), we find

$$\begin{aligned}\phi_{ij}(\kappa_1,\kappa_2;z,z') &= \int_{-\infty}^{\infty}\Big[\, e^{i\kappa_3(z'-z)}\Phi_{ij}^{(H)}(\boldsymbol{\kappa}) \\ &+ e^{-i\kappa_3 z-\kappa_h z'} m_j(\kappa_1,\kappa_2)\Phi_{i3}^{(H)}(\boldsymbol{\kappa}) \\ &+ e^{i\kappa_3 z'-\kappa_h z} m_i^*(\kappa_1,\kappa_2)\Phi_{3j}^{(H)}(\boldsymbol{\kappa}) \\ &+ e^{-\kappa_h(z+z')} m_i^*(\kappa_1,\kappa_2)m_j(\kappa_1,\kappa_2)\Phi_{33}^{(H)}(\boldsymbol{\kappa})\Big]\, d\kappa_3. \end{aligned} \tag{B-6}$$

The integrations can be calculated explicitly, with the Fourier transform relation

$$\phi_{ij}^{(H)}(\kappa_1,\kappa_2;r_3) = \int_{-\infty}^{\infty}\Phi_{ij}^{(H)}(\boldsymbol{\kappa})\exp(i\kappa_3 r_3)\, d\kappa_3. \tag{B-7}$$

The result of performing these integrations is equation (3.12). Hence, Hunt and Graham's result is indeed equivalent to the result in this report.

References

Batchelor, G. K. (1953): *The Theory of Homogeneous Turbulence.* Cambridge Univ. Press, Cambridge, Great Britain.

Bendat, J. S., and A. G. Piersol (1986): *Random Data: Analysis and Measurement Procedures.* Wiley-Interscience, New York.

Caughey, S. J., and S. G. Palmer (1979): Some aspects of turbulence structure through the depth of the convective boundary layer. *Q. J. R. Meteorol. Soc.*, **105**, 811–827.

Corrsin, S. (1964): Further generalizations of Onsager's cascade model for turbulent spectra. *Phys. Fluids*, **7**, 1156–1159.

Davenport, A. G. (1961): The spectrum of horizontal gustiness near the ground in high winds. *Q. J. R. Meteorol. Soc.*, **100**, 572–592.

Gradshteyn, I. S., and I. M. Ryzhik (1994): *Table of Integrals, Series, and Products.* Academic Press, San Diego.

Højstrup, J. (1982): Velocity spectra in the unstable planetary boundary layer. *J. Atmos. Sci.*, **39**, 2239–2248.

Hunt, J.C.R. (1984): Turbulence structure in thermal convection and shear-free boundary layers. *J. Fluid Mech.*, **138**, 161–184.

Hunt, J.C.R., and J.M.R. Graham (1978): Free-stream turbulence near plane boundaries. *J. Fluid Mech.*, **84**, 209–235.

Hunt, J.C.R., J. C. Kaimal, and J. E. Gaynor (1988): Eddy structure in the convective boundary layer—new measurements and new concepts. *Q. J. R. Meteorol. Soc.*, **114**, 827–858.

Kaimal, J. C. (1978): Horizontal velocity spectra in an unstable surface layer. *J. Atmos. Sci.*, **35**, 18–24.

Kaimal, J. C., J. C. Wyngaard, D. A. Haugen, O. R. Coté, and Y. Izumi (1976): Turbulence structure in the convective boundary layer. *J. Atmos. Sci.*, **33**, 2152–2169.

Kaimal, J. C., J. C. Wyngaard, Y. Izumi, and O. R. Coté (1972): Spectral characteristics of surface layer turbulence. *Q. J. R. Meteorol. Soc.*, **98**, 563–589.

Kolmogorov, A. N. (1941): The local structure of turbulence in incompressible viscous fluid for very large Reynolds numbers. *C. R. Acad. Sci. URSS*, **30**, 301–305.

Kristensen, L., D. H. Lenschow, P. Kirkegaard, and M. Courtney (1989): The spectral velocity tensor for homogeneous boundary-layer turbulence. *Bound. Layer Meteorol.*, **47**, 149–193.

Lenschow, D. H., and B. B. Stankov (1986): Length scales in the convective boundary layer. *J. Atmos. Sci.*, **43**, 1198–1209.

Mann, J. (1994): The spatial structure of neutral atmospheric surface layer turbulence. *J. Fluid Mech.*, **273**, 141–168.

Moeng, C.-H. (1984): A large-eddy-simulation model for the study of planetary boundary-layer turbulence. *J. Atmos. Sci.*, **41**, 2052–2062.

Panofsky, H. A., and J. A. Dutton (1984): *Atmospheric Turbulence: Models and Methods for Engineering Applications.* Wiley & Sons, New York.

Peltier, L. J., J. C. Wyngaard, S. Khanna, and J. Brasseur (1996): Spectra in the unstable surface layer. *J. Atmos. Sci.*, **53**, 44–61.

Soucy, R., R. Woodward, and H. A. Panofsky (1982): Vertical cross-spectra of horizontal velocity components at the Boulder Observatory. *Bound. Layer Meteorol.*, **24**, 57–66.

Tennekes, H., and J. L. Lumley (1972): *A First Course in Turbulence.* MIT Press, Cambridge, Mass.

von Kármán, T. (1948): Progress in the statistical theory of turbulence. *Proc. Nat. Acad. Sci.*, **34**, 530–539.

Wyngaard, J. C., O. R. Coté, and Y. Izumi (1971): Local free convection, similarity, and the budgets of shear stress and heat flux. *J. Atmos. Sci.*, **28**, 1171–1182.

Acronyms

1D, 2D, 3D	one-, two-, or three-dimensional
AMTEX	Air Mass Transformation Experiment
CBL	convective boundary layer
FFT	fast Fourier transform
LES	large-eddy simulation
TKE	turbulent kinetic energy

Distribution

Admnstr
Defns Techl Info Ctr
Attn DTIC-OCP
8725 John J Kingman Rd Ste 0944
FT Belvoir VA 22060-6218

Mil Asst for Env Sci
Ofc of the Undersec of Defns for Rsrch & Engrg R&AT E LS
Pentagon Rm 3ED129
Washington DC 20301-3080

Ofc of the Secy of Defs
Attn ODDRE (R&AT) G Singley
Attn ODDRE (R&AT) S Gontarek
The Pentagon
Washington DC 20301-3080

ARL Chemical Biology Nuc Effects Div
Attn AMSRL-SL-CO
Aberdeen Proving Ground MD 21005-5423

Army ARDEC
Attn SMCAR-IMI-I
BLDG 59
Dover NJ 07806-5000

Army Communications Elec Ctr for EW RSTA
Attn AMSEL-EW-D
Attn AMSEL-EW-MD
FT Monmouth NJ 07703-5303

Army Corps of Engrg
Attn ETL-GS-LB
FT Belvoir VA 22060

Army Dugway Proving Ground
Attn STEDP 3
Attn STEDP-MT-DA-L-3
Attn STEDP-MT-M Bowers
Dugway UT 84022-5000

Army Field Artillery School
Attn ATSF-TSM-TA
FT Sill OK 73503-5000

Army Foreign Sci Tech Ctr
Attn CM
220 7th Stret NE
Charlottesville VA 22901-5396

Army Infantry
Attn ATSH-CD-CS-OR E Dutoit
FT Benning GA 30905-5090

Army Materiel Sys Analysis Activity
Attn AMXSY H Cohen
Attn AMXSY-AT Campbell
Attn AMXSY-CR Marchet
Attn AMXSY-CS Bradley
Aberdeen Proving Ground MD 21005-5071

Army Missile Cmnd
Attn AMSMI-RD-CS-R Doc
Redstone Arsenal AL 35898-5241

Army Missile Cmnd
Attn AMSMI-RD-AC-AD Peterson
Redstone Arsenal AL 35898-5242

Army Missile Cmnd
Attn AMSMI-RD-DE-SE G Lill Jr
Redstone Arsenal AL 35898-5245

Army Missile Cmnd
Attn AMSMI-RD-AS-SS H F Anderson
Attn AMSMI-RD-AS-SS B Williams
Redstone Arsenal AL 35898-5253

Army Nuclear Cml Agency
Attn MONA ZB
Bldg 2073
Springfield VA 22150-3198

Army OEC
Attn CSTE EFS
4501 Ford Ave Park Center IV
Alexandria VA 22302-1458

Army Rsrch Ofc
Attn AMXRO-GS Bach
PO Box 12211
Research Triangle Park NC 27709

Army Satellite Comm Agcy
Attn DRCPM SC 3
FT Monmouth NJ 07703-5303

Army Strat Defns Cmnd
Attn CSSD-SL-L Lilly
PO Box 1500
Huntsville AL 35807-3801

Distribution

Army Topo Engr Ctr
Attn CETEC-ZC-1
FT Belvoir VA 22060-5546

CECOM
Attn PM GPS COL S Young
FT Monmouth NJ 07703

CECOM RDEC Electronic Systems Div Dir
Attn J Niemela
FT Monmouth NJ 07703

CECOM
Sp & Terrestrial Commctn Div
Attn AMSEL-RD-ST-MC-M H Soicher
FT Monmouth NJ 07703-5203

DARPA
Attn B Kaspar
Attn J Pennella
Attn L Stotts
3701 N Fairfax Dr
Arlington VA 22203-1714

Dpty Assist Scy for Rsrch & Techl
Attn SARD-TR R Chait Rm 3E476
Attn SARD-TT D Chait
Attn SARD-TT F Milton Rm 3E479
Attn SARD-TT K Kominos
Attn SARD-TT R Reisman
Attn SARD-TT T Killion
The Pentagon
Washington DC 20310-0103

DUSD Space
Attn 1E765 J G McNeff
3900 Defense Pentagon
Washington DC 20301-3900

Hdqtrs Dept of the Army
Attn DAMO-FDQ D Schmidt
400 Army Pentagon
Washington DC 20310-0460

Kwajalein Missile Range
Attn Meteorologist in Charge
PO Box 57
APO San Francisco CA 96555

Logistics Ctr
Attn ATCL-CE
FT Lee VA 23801-6000

Natl Security Agency
Attn W21 Longbothum
9800 Savage Rd
FT George G Meade MD 20755-6000

Naval Air Dev Ctr
Attn Code 5012 A Salik
Warminister PA 18974

OSD
Attn OUSD(A&T)/ODDDR&E(R) J Lupo
The Pentagon
Washington DC 20301-7100

US Army Matl Cmnd
Dpty CG for RDE Hdqtrs
Attn AMCRD BG Beauchamp
5001 Eisenhower Ave
Alexandria VA 22333-0001

US Army Matl Cmnd
Prin Dpty for Acquisition Hdqrts
Attn AMCDCG-A D Adams
5001 Eisenhower Ave
Alexandria VA 22333-0001

US Army Matl Cmnd
Prin Dpty for Techlgy Hdqrts
Attn AMCDCG-T M Fisette
5001 Eisenhower Ave
Alexandria VA 22333-0001

US Army TRADOC Anlys Cmnd—WSMR
Attn ATRC-WSS-R
White Sands Missile Range NM 88002

US Military Academy
Dept of Mathematical Sci
Attn MAJ D Engen
West Point NY 10996

USAASA
Attn MOAS-AI W Parron
9325 Gunston Rd Ste N319
FT Belvoir VA 22060-5582

USACRREL
Attn CEREL-GP R Detsch
72 Lyme Rd
Hanover NH 03755-1290

Distribution

USATRADOC
Attn ATCD-FA
FT Monroe VA 23651-5170

Nav Air War Cen Wpn Div
Attn CMD 420000D C0245 A Shlanta
1 Admin Cir
China Lake CA 93555-6001

Naval Surface Weapons Ctr
Attn Code G63
Dahlgren VA 22448-5000

AFMC DOW
Wright Patterson AFB OH 45433-5000

Air Weather Service
Attn Tech Lib FL4414 3
Scott AFB IL 62225-5458

Dept of the Air Force
Attn OL A 2D Weather squad Mac
Holloman AFB NM 88330-5000

GPS Joint Prog Ofc Dir
Attn COL J Clay
2435 Vela Way Ste 1613
Los Angeles AFB CA 90245-5500

Hdqtrs AWS DOO 1
Scott AFB IL 62225-5008

Ofc of the Dir Rsrch and Engrg
Attn R Menz
Pentagon Rm 3E1089
Washington DC 20301-3080

Phillips Lab Atmospheric Sci Div
Geophysics Dirctrt
Hanscom AFB MA 01731-5000

Phillips Laboratory
Attn PL/LYP Chisholm
Hanscom AFB MA 01731-5000

Special Assist to the Wing Cmndr
Attn 50SW/CCX CAPT P H Bernstein
300 O'Malley Ave Ste 20
Falcon AFB CO 80912-3020

USAF Rome Lab Tech
Attn Corridor W Ste 262 RL SUL
26 Electr Pkwy Bldg 106
Griffiss AFB NY 13441-4514

USAF SMC/CED
Attn DMA/JPO M Ison
2435 Vela Way Ste 1613
Los Angeles AFB CA 90245-5500

USAFETAC DNE
Attn Glauber
Scott AFB IL 62225-5008

Nasa Marshal Space Flt Ctr
Atmospheric Sciences Div
Attn E501 Fichtl
Huntsville AL 35802

Nasa Spct Flt Ctr
Atmospheric Sciences Div
Attn Code ED 41 1
Huntsville AL 35812

ARL Electromag Group
Attn Campus Mail Code F0250 A Tucker
University of TX
Austin TX 78712

Dept of Commerce Ctr
Mountain Administration
Attn Spprt Ctr Library R51
325 S Broadway
Boulder CO 80303

Lockheed Missile & Spc Co
Attn Org 91 01 B 255 K R Hardy
3251 Hanover Stret
Palo Alto CA 94304-1191

Natl Ctr for Atmospheric Research
Attn NCAR Library Serials
PO Box 3000
Boulder CO 80307-3000

NCSU
Attn J Davis
PO Box 8208
Raleigh NC 27650-8208

Distribution

NTIA ITS S3
Attn H J Liebe
325 S Broadway
Boulder CO 80303

Pacific Missile Test Ctr Geophysics Div
Attn Code 3250
Point Mugu CA 93042-5000

Army Rsrch Laboratory
Attn AMSRL-BE-S Battlefield Envir Dir
Attn AMSRL-BE-W
White Sands Missile Range NM 88002-5501

US Army Rsrch Lab
Attn AMSRL-CI-LL Tech Lib (3 copies)
Attn AMSRL-CS-AL-TA Mail & Records Mgmt
Attn AMSRL-CS-AL-TP Techl Pub (3 copies)
Attn AMSRL-IS-EE D K Wilson (15 copies)
Attn AMSRL-SE-EE Z G Sztankay
Adelphi MD 20783-1197

REPORT DOCUMENTATION PAGE

Form Approved
OMB No. 0704-0188

1. AGENCY USE ONLY *(Leave blank)*	2. REPORT DATE	3. REPORT TYPE AND DATES COVERED
	July 1997	Final, 1 February 1996 to 30 April 1996

4. TITLE AND SUBTITLE
Three-Dimensional Correlation and Spectral Functions for Turbulent Velocities in Homogeneous and Surface-Blocked Boundary Layers

5. FUNDING NUMBERS
DA PR: B53A
PE: P61102

6. AUTHOR(S)
David Keith Wilson

7. PERFORMING ORGANIZATION NAME(S) AND ADDRESS(ES)
U.S. Army Research Laboratory
Attn: AMSRL-IS-EE
2800 Powder Mill Road
Adelphi, MD 20783-1197

8. PERFORMING ORGANIZATION REPORT NUMBER
ARL-TR-1287

9. SPONSORING/MONITORING AGENCY NAME(S) AND ADDRESS(ES)
U.S. Army Research Laboratory
2800 Powder Mill Road
Adelphi, MD 20783-1197

10. SPONSORING/MONITORING AGENCY REPORT NUMBER

11. SUPPLEMENTARY NOTES
AMS code: 61102.53A11
ARL PR: 7FEJ60

12a. DISTRIBUTION/AVAILABILITY STATEMENT
Approved for public release; distribution unlimited.

12b. DISTRIBUTION CODE

13. ABSTRACT *(Maximum 200 words)*

A pair of three-dimensional (3D) models for correlation functions and spectra of velocity fluctuations in turbulent boundary layers is presented. First, the case of homogeneous turbulence is considered. Von Kármán's energy spectrum is used to develop a complete set of 3D correlation and spectral equations. Second, it is shown how the homogeneous spectra can be modified to include the effect of eddy-blocking at the ground. Assuming that the disturbance to the turbulent flow resulting from the blocking is irrotational, an equation is developed that allows one to write the vertically inhomogeneous, 2D cross spectra as a function of the 2D cross spectra for a homogeneous flow. Although there are only two adjustable parameters in the inhomogeneous model, the variance and a length scale, the model is shown to agree quite well with a variety of previous results for the atmospheric convective boundary layer (CBL).

14. SUBJECT TERMS
turbulence, atmosphere, boundary layers, spectra

15. NUMBER OF PAGES
49

16. PRICE CODE

17. SECURITY CLASSIFICATION OF REPORT	18. SECURITY CLASSIFICATION OF THIS PAGE	19. SECURITY CLASSIFICATION OF ABSTRACT	20. LIMITATION OF ABSTRACT
Unclassified	Unclassified	Unclassified	UL

NSN 7540-01-280-5500

Standard Form 298 (Rev. 2-89)
Prescribed by ANSI Std. Z39-18
298-102